BRNO UNIVERSITY OF TECHNOLOGY

Faculty of Electrical Engineering
and Communication

MASTER'S THESIS

Brno, 2021 Bc. Tereza Smejkalová

BRNO UNIVERSITY OF TECHNOLOGY

VYSOKÉ UČENÍ TECHNICKÉ V BRNĚ

FACULTY OF ELECTRICAL ENGINEERING AND COMMUNICATION

FAKULTA ELEKTROTECHNIKY
A KOMUNIKAČNÍCH TECHNOLOGIÍ

DEPARTMENT OF ELECTRICAL AND ELECTRONIC TECHNOLOGY

ÚSTAV ELEKTROTECHNOLOGIE

ENERGY DISPERSIVE X-RAY SPECTROSCOPY OF DOPED PVDF FIBERS

ENERGETICKY DISPERZNÍ RENTGENOVÁ SPEKTROSKOPIE DOPOVANÝCH VLÁKEN PVDF

MASTER'S THESIS
DIPLOMOVÁ PRÁCE

AUTHOR
AUTOR PRÁCE

Bc. Tereza Smejkalová

SUPERVISOR
VEDOUCÍ PRÁCE

Mgr. Dinara Sobola, Ph.D.

BRNO 2021

BRNO UNIVERSITY OF TECHNOLOGY
FACULTY OF ELECTRICAL ENGINEERING AND COMMUNICATION

Master's Thesis

Master's study program **Electrical Manufacturing and Management**

Department of Electrical and Electronic Technology

Student: Bc. Tereza Smejkalová ***ID:*** 195250

Year of study: 2 ***Academic year:*** 2020/21

TITLE OF THESIS:

Energy dispersive X-ray spectroscopy of doped PVDF fibers

INSTRUCTION:

Study correlation between composition from EDX analysis and electrical performance of doped PVDF fibers.

RECOMMENDED LITERATURE:

D. Lolla, et. al. Polarized Catalytic Polymer Nanofibers. Materials 2019, 12(18), 2859.

K. Castkova, et. al. Structure–Properties Relationship of Electrospun PVDF Fibers. Nanomaterials 2020, 10(6), 1221.

Date of project specification: 8.2.2021 ***Deadline for submission:*** 24.5.2021

Supervisor: Mgr. Dinara Sobola, Ph.D.

doc. Ing. Petr Bača, Ph.D.
Chair of study program board

Abstract

This diploma thesis focuses on a flexible energy harvesting system based on piezoelectric polymer polyvinylidene fluoride (PVDF) with an emphasis on manipulating and optimising the properties and performance. By incorporating powders of piezo-active ceramics, the properties of piezoelectric polymer PVDF could be significantly improved and converted into useful electrical energy. PVDF was formed by electrospinning into fibres with a thickness of 1.5-0.3 μm and then studied with various analytical methods. This work offers a description of electrospinning, a preparation of samples for examination and a theoretical introduction to the analytical methods to which the samples were subjected. The morphology and distribution of the nanostructured ceramics into the PVDF polymer matrix was observed by scanning electron microscopy (SEM) and energy-dispersive X-ray spectroscopy (EDX). For the formation of β phase and detailed phase composition, the samples were comprehensively characterised by Fourier transform infrared spectroscopy (FTIR). The work also contains analysis in Raman spectroscopy, a method used to identify and compare chemical compounds. The electrical characteristics were studied by dielectric spectroscopy and the correlation with composition is provided. Individual components of doped fibres are characterised and discussed relating to their future use in sensors.

Keywords

polymer, ceramics, nanofibre, nanocomposite, piezoelectricity, polyvinylidene fluoride, electroactive phase, electrospinning, SEM, EDX, FTIR, Raman, dielectric constant

Abstrakt

Tato diplomová práce zkoumá flexibilní materiál k produkci elektřiny založený na piezoelektrickém polymeru Polyvinylidenfluorid (PVDF). Inkorporací piezoaktivní keramiky lze vlastnosti piezoelektrického polymeru PVDF významně zlepšit a převést na užitečnou elektrickou energii. PVDF byl vytvořen elektrostatickým zvlákňováním do vláken o tloušťce 1,5-0,3 μm a poté studován různými analytickými metodami. Tato práce nabízí popis elektrostatického zvlákňování, přípravu vzorků a teoretický úvod do analytických metod, kterým byly vzorky podrobeny. Morfologie a distribuce nanostrukturované keramiky do polymerní matrice PVDF byla pozorována použitím skenovací elektronové mikroskopie (SEM) a energiově disperzní spektroskopie (EDX). Pro tvorbu β fáze a podrobné fázové složení byly vzorky charakterizovány infračervenou spektroskopií s Fourierovou transformací (FTIR). Práce také obsahuje analýzu s použitím Ramanovy spektroskopie, metody používané k identifikaci a porovnání chemických sloučenin. Elektrické vlastnosti byly studovány dielektrickou spektroskopií a je poskytnuta korelace se složením. Jednotlivé komponenty dotovaných vláken jsou charakterizovány a vyhodnocovány v souvislosti s jejich budoucím využitím v senzorech.

Klíčová slova

polymer, keramika, nanovlákno, nanokompozit, piezoelektřina, polyvinylidenfluorid, elektroaktivní fáze, elektrostatické zvlákňování, SEM, EDX, FTIR, Raman, permitivita

Rozšířený abstrakt

Piezoelektrické materiály jsou jedinečné materiály, které generují elektrický náboj v reakci na aplikované napětí nebo mírnou mechanickou deformaci, čímž eliminují potřebu externích zdrojů energie pro elektrickou stimulaci. Polyvinyliden fluorid (PVDF) je semikrystalický polymer s piezoelektrickými vlastnostmi, mající pět krystalických polymorfů, včetně α-, β-, γ-, δ- a ε-fází v závislosti na podmínkách krystalizace a zpracování. Jeho molekulární řetězec se skládá z vysoce elektronegativních atomů fluoru ve srovnání s atomy uhlíku a vodíku. Vede k tvorbě polárních vazeb C-F a každá vazba C-F má významný dipólový moment. Polyvinyliden fluorid je jedním z nejslibnějších elektroaktivních polymerů; vykazuje vynikající elektroaktivní chování, dobrou biokompatibilitu, vynikající chemickou odolnost a tepelnou stabilitu, což z něj činí atraktivní materiál pro biomedicínské, elektronické, environmentální i energetické aplikace. Tato práce si klade za cíl dále vylepšit jeho vlastnosti inkluzí prášků piezoaktivních materiálů.

Diplomová práce nabízí popis postupu v přípravě vzorků, charakterizuje jednotlivé složky dopovaných vláken a věnuje se i konkrétním analytickým metodám včetně použitých přístrojů. Získané znamenité vlastnosti dopovaného PVDF by mohly být použity při návrhu senzorů.

Bibliographic citation

SMEJKALOVÁ, Tereza. Energeticky disperzní rentgenová spektroskopie dopovaných vláken PVDF [online]. Brno, 2020 [cit. 2020-12-18]. Dostupné z: https://www.vutbr.cz/studenti/zav-prace/detail/131971. Semestrální práce. Vysoké učení technické v Brně, Fakulta elektrotechniky a komunikačních technologií, Ústav elektrotechnologie. Vedoucí práce Dinara Sobola.

Author's Declaration

Author:	*Tereza Smejkalová*
Author's ID:	*195250*
Paper type:	*Master's Thesis*
Academic year:	*2020/21*
Topic:	*Energy dispersive X-ray spectroscopy of doped PVDF fibers*

I declare that I have written this paper independently, under the guidance of the advisor and using exclusively the technical references and other sources of information cited in the project and listed in the comprehensive bibliography at the end of the project.

As the author I furthermore declare that, with respect to the creation of this paper, I have not infringed any copyright or violated anyone's personal and/or ownership rights. In this context, I am fully aware of the consequences of breaking Regulation § 11 of the Copyright Act No. 121/2000 Coll. of the Czech Republic, as amended, and of any breach of rights related to intellectual property or introduced within amendments to relevant Acts such as the Intellectual Property Act or the Criminal Code, Act No. 40/2009 Coll., Section 2, Head VI, Part 4.

Brno, May 24, 2021 ----------

author's signature

Acknowledgement

First of all, I would like to express my appreciation and thanks to my supervisor Mgr. Dinara Sobola, Ph.D., for her professional guidance and valuable advice in processing this work. Her tremendous work towards contribution to science is inspiring for all people who meet her. Special thanks go to Bc. Filip Šmatlo for all the valuable discussions, support, and patience. My gratitude goes to my entire family, especially my parents, who always supported and encouraged my studies over the years.

The research described in this work was supported by the Grant Agency of Czech Republic under project No. 19-17457S. A part of the work was carried out with the support of CEITEC Nano Re-search Infrastructure [grant ID LM2015041, MEYS CR, 2016–2019], CEITEC Brno University of Technology.

Brno, May 23, 2021 ----------

author's signature

Contents

1. MATERIAL OF FIBRES 11

1.1 PIEZOELECTRICITY 11
1.2 POLYVINYLIDENE FLUORIDE 12
1.3 PIEZOELECTRIC CERAMICS 13
1.3.1 BCZT 14
1.3.2 BT 14
1.3.3 KNN 14
1.3.4 TiO_2 14
1.3.5 ZnO 15

2. PREPARATION OF DOPED PVDF FIBRES 16

2.1 CONTIPRO 4SPIN LAB 17

3. ANALYSIS OF DOPED PVDF FIBRES 18

3.1 SCANNING ELECTRON MICROSCOPY (SEM) 18
3.1.1 SEM microscope Tescan Lyra 3 20
3.1.2 Sample Preparation 20
3.1.3 SEM images of samples 22
3.2 ENERGY DISPERSIVE X-RAY SPECTROSCOPY (EDX) 24
3.2.1 EDX micrographs of Samples 25
3.3 FOURIER TRANSFORM INFRARED SPECTROSCOPY (FTIR) 31
3.3.1 Device for FTIR analysis VERTEX 70v 32
3.3.2 FTIR analysis of samples 32
3.4 RAMAN SPECTROSCOPY 36
3.4.1 Raman Microscope Alpha300 R 37
3.4.2 Raman analysis of samples 38
3.5 MEASURING OF DIELECTRIC CONSTANT 40

4. CONCLUSION 43

FIGURES

1.1 Direct and converse piezoelectric effect 11
1.2 (a) A barium titanate unit cell showing the displacement of Ti 4+ in the TiO 6 octahedra (b) Physical interpretation of the dipole due to the non-centrosymmetric structure of unit cell [8] 12
1.3 Structures of α, β, and γ phase polyvinylidene fluoride (PVDF) [11] 13
2.1 a) Electrospinning device Contipro 4SPIN LAB with needle emitter and rotating collector b) Polymer solution in a dispenser 17
3.1 Scanning electron microscope [33] 18
3.2 Scanning electron microscope Tescan Lyra 3 20
3.3 a) Coater Leica EM ACE600 b) Coated samples in holders 21
3.4 Coater Leica EM ACE600 a) Carbon thread aperture b) Changing of carbon thread 22
3.5 Sem micrograph of PVDF/BCZT composite with a field view a) 20μm b) 10μm 22
3.6 Sem micrograph of PVDF/BT composite with field view a) 20μm b) 10μm 23
3.7 Sem micrograph of PVDF/KNN composite with field view a) 20μm b) 10μm 23
3.8 Sem micrograph of PVDF/TiO_2 composite with field view a) 20μm b) 10μm 23
3.9 Sem micrograph of PVDF/ZnO composite with field view a) 20μm b) 10μm 24
3.10 PVDF/BCZT composite with field view 3 μm 25
3.11 PVDF/BT composite with field view 6 μm 26
3.12 PVDF/KNN composite with field view 2 μm 26
3.13 PVDF/TiO_2 composite with field view 2 μm 27
3.14 PVDF/ZnO composite with field view 3 μm 27
3.15 EDX spectrum of PVDF fibres doped by BCZT 28
3.16 EDX spectrum of PVDF fibres doped by BT 29
3.17 EDX spectrum of PVDF fibres doped by KNN 29
3.18 EDX spectrum of PVDF fibres doped by TiO_2 30
3.19 EDX spectrum of PVDF fibres doped by ZnO 30
3.20 Schematic diagram depicting the optical components of the FTIR system similar to the system used in this thesis but enriched for AFM-Cantilever. [46] 31
3.21 FTIR spectroscope VERTEX 70v 32
3.22 FTIR spectrum of PVDF fibres doped by BCZT 33
3.23 FTIR spectrum of PVDF fibres doped by BT 33
3.24 FTIR spectrum of PVDF fibres doped by KNN 34
3.25 FTIR spectrum of PVDF fibres doped by TiO_2 34
3.26 FTIR spectrum of PVDF fibres doped by ZnO 35
3.27 The experimental scheme for the Raman-spectroscopy-based concentration sensor (RCS) [55] 36
3.28 Raman Microscope Alpha300 R 37
3.29 Raman spectra of PVDF doped by barium calcium zirconate titanate (BCZT) 38
3.30 Raman spectra of PVDF doped by barium titanate (BT) 38
3.31 Raman spectra of PVDF doped by potassium sodium niobate (KNN) 39
3.32 Raman spectra of PVDF doped by titanium dioxide (TiO_2) 39
3.33 Raman spectra of PVDF doped by zinc oxide (ZnO) 39
3.34 Alpha-A High Performance Frequency Analyser 40
3.35 Progress of relative permittivity of PVDF/BCZT nanocomposite in the frequency range 1-100 kHz 41
3.36 Progress of relative permittivity of PVDF/BT nanocomposite in the frequency range 1-100 kHz 41
3.37 Progress of relative permittivity of PVDF/TiO_2 nanocomposite in the frequency range 1-100 kHz 42
3.38 Progress of relative permittivity of PVDF/ZnO nanocomposite in the frequency range 1-100 kHz 42

TABLES

2.1 The electrospinning processing parameters for manufacturing PVDF fibres doped by piezoelectric ceramics.....17
3.1 Fourier Transform Infrared Spectroscopy (FTIR) phase calculation 35
3.2 Measurement of relative permittivity (ε_r).....40

INTRODUCTION

With the advent of nanotechnology, it is possible to create materials with a diverse range of properties. The modification of materials principally provides additional features and aptitudes while maintaining the fundamental characteristics of the materials. In this thesis, polymer fibres were enriched with nano-sized particles of piezo-active ceramics.

Piezoelectric and pyroelectric materials are particularly advantageous for a variety of energy harvesting applications. 'The concept of harvesting energy covers applications that produce relatively small levels of power (nW to mW) from mechanical loads, vibrations, human motion, waste heat, light or chemical sources.' The power generated by the harvesting material or device is used for low-power electronics, lighting, or wireless sensor systems. Autonomous self-powered systems are not dependent on power cables or batteries - resulting in environmental benefits from reduced battery usage.

Polymer nanocomposites are composite materials in which nano-sized fillers are dispersed in the polymer matrix. Incorporating a small number of suitable nanoscale fillers offers the creation of composite materials with superior properties and additional functionalities. Moreover, resulting fibres of polymer-based nanocomposites demonstrate high breakdown strength and can produce some of the strongest materials known [1]. This phenomenon is caused by stretching a macromolecular system into a fibre, which orients the polymer chains and increases intermolecular interactions. Different nanostructured ceramic-based materials like, especially, lead zirconate titanate Pb (Zr, Ti)O_3 (PZT) and barium titanate ($BaTiO_3$) have already been investigated to improve dielectric constant as a composite with organic polymers as a matrix due to their great potentials as better energy harvesters with higher volume efficiency.

Creating those complex structures can only be controlled if we understand the nature of the processes [2]. These advanced processes and their outcomes are the focus of this text.

The electroactive material used in this thesis is polyvinylidene fluoride (PVDF). Flexible electroactive materials are in high demand in electronic applications such as sensors, actuators or energy harvesting devices. Materials like PVDF attracted research attention not only for their flexibility but also due to their outstanding pyroelectricity, piezoelectricity, triboelectricity and ferroelectricity, as well as their relatively high dielectric permittivity [3]. Additionally, it is possible to obtain a high dielectric constant by doping PVDF with ceramic particles. Polymers possess good processability, mechanical flexibility and low cost but have a minimal value of dielectric constant to be useful as capacitors. Therefore, polymer-ceramic composites can be an excellent choice to achieve the miniaturisation of energy storage devices by combining the merits of polymers and ceramics [4].

1. MATERIAL OF FIBRES

1.1 Piezoelectricity

Piezoelectric materials are unique materials eliminating the need for external power sources for electrical stimulation. Piezoelectric materials either generate an electric charge in response to mechanical stress or generate mechanical work when electric charge is applied. When a piezoelectric is strained with external stress, its charges displace from their equilibrium position, causing bound charges on the surface. This effect is the direct piezoelectricity, and its mechanism is shown in Fig. 1a. The piezoelectric effect is a reversible process – when an external electric field induces elastic displacement of charges, the material stretches. The produced elongation is proportional to the charge density, and the mechanism of the converse piezoelectricity is shown in Fig. 1.1.

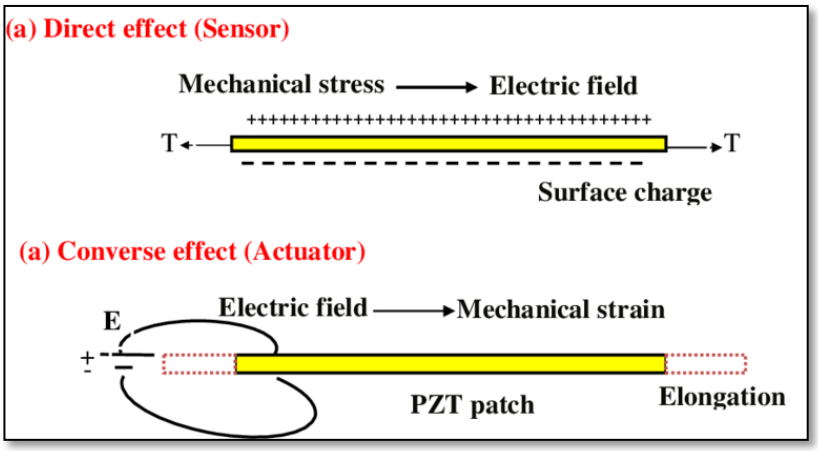

Fig. 1.1 Direct and converse piezoelectric effect

Piezoelectric effect is possible due to unit cell houses and a permanent dipole of materials similar to barium titanate. Barium, titanium and oxygen ions possess a unique non-symmetric positioning in the tetragonally shaped unit cell, see Fig. 1.2. As explained by Ashwini Bharathula [5], each titanium ion in the barium itanate molecule is surrounded by an octahedral order of oxygen ions but is slightly displaced from the centre of the octahedron. This charge separation induces a permanent dipole - permanent dipole describes the partial charge separation that can occur within a molecule along the bond that forms between two different atoms. 'However, different groups of dipoles are usually randomly oriented across the material and cancel each other out.' [5, p. 1] Therefore, materials like Barium titanate must be subjected to additional processing called poling to re-orient the dipoles - making extracting useful piezoelectricity possible. During poling, the material is being heated and simultaneously exposed to an electric field. Due to this process, many dipoles in the material become oriented in a preferred direction. After the heating, the material is “frozen” and can keep the position of its electric dipoles for a long

period of time [6]. ‘After this stage, a mechanical force applied in an appropriate direction can increase the existing voltage by thousands of volts.' [5, p. 1]

Typical piezoelectric materials include barium titanate, lead titanate and lead zirconate titanate ceramics as well as electroactive polymers such as polyvinylidene fluoride (PVDF) [7].

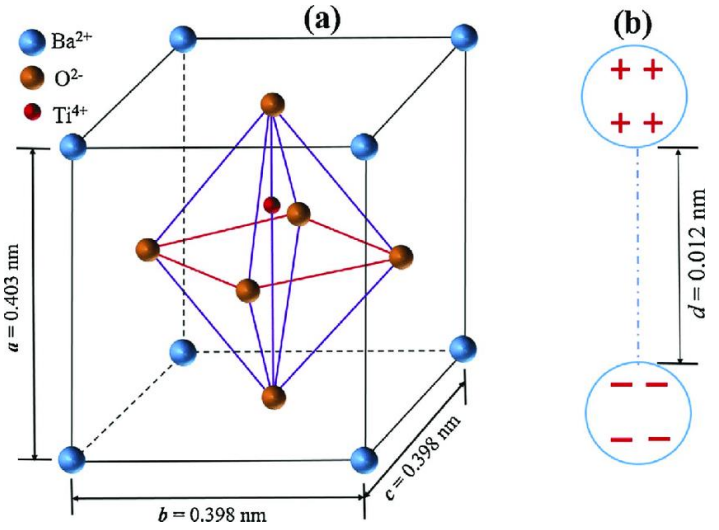

Fig. 1.2 (a) A barium titanate unit cell showing the displacement of Ti 4+ in the TiO 6 octahedra (b) Physical interpretation of the dipole due to the non-centrosymmetric structure of unit cell [8]

1.2 Polyvinylidene Fluoride

Piezoelectric polymers exhibit several advantages making it suitable for biomedical, electronic, environmental and energy harvesting applications [7]. PVDF exhibits excellent electroactive behaviours, good biocompatibility, excellent chemical resistance, and thermal stability [9].

PVDF is a semicrystalline polymer having five crystalline polymorphs, including α-, β-, γ- δ- and ε-phases depending on the crystallization and processing conditions. Its molecular chain consists of highly electronegative fluorine atoms compared to the carbon and hydrogen atoms, see Fig. 1.3. It leads to the formation of polar C–F bonds, and each C–F bond possesses a significant dipole moment [7]. Polar β-phase, as explained by J. Y. Lim, S. Kim and Y. Seo, has all of its dipoles aligned in the same direction normal to the chain axis. Its unit cell consists of two all-trans chains packed with their dipoles pointing in the same direction. The molecular dipoles in the β-phase are thus entirely aligned in one direction; this crystal form can consequently generate the largest spontaneous polarisation and exhibits strong ferroelectric and piezoelectric properties [10].

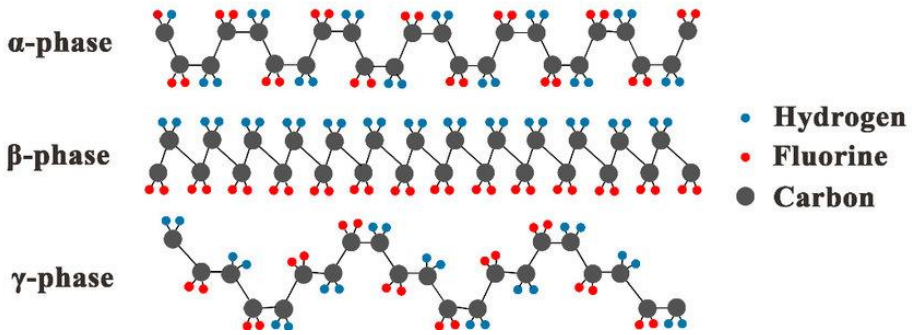

Fig. 1.3 Structures of α, β, and γ phase polyvinylidene fluoride (PVDF) [11]

These unique β-phase properties of PVDF make it useful in a wide range of applications, including actuators, biosensor, energy harvesting materials, audio devices, transducers, and non-volatile memories [12]. The β-phase can be promoted in PVDF by either mechanical drawing, annealing, electrical poling, or nanoparticle additions [13]. A wide variety of synthesis and processing methods allow the production of materials whose electrical properties include different conductivity, capacitance, or dielectric strength.

Polymer-based nanocomposites have attracted interest for numerous reasons. For instance, organic polymers possess small dielectric permittivity, whereas ceramics have large permittivity. However, ceramic particles are brittle - they have a low breakdown strength and are difficult to process. Ceramic-polymer composites offer an opportunity to design a material with excellent dielectric and mechanical properties and provide a complementary effect of the high dielectric permittivity (due to ceramics) and elasticity, flexibility, and high breakdown strength and lightweight (due to organic polymers).

Numerous nanomaterials can be synthesized for biomedical and industrial applications - in particular, clay nanoplatelets, carbon nanotubes, graphene/graphene oxide and piezoelectric ceramics have been reported to be very effective to induce β-phase in PVDF [14].

1.3 Piezoelectric Ceramics

In recent years, researchers have been interested in developing lead-free piezoelectric materials as alternatives to lead-based materials, such as $(K0.5Na0.5)NbO_3$ (KNN), $(Na_{0.5}Bi_{0.5})TiO_3$ (NBT), $(BaZr_xTi_{(1-x)}O_3$ (BZT) and $Ba_{(1-x)}Ca_xTiO_3$ (BCT). Various nanostructured ceramic–based materials like lead zirconate titanate $Pb(Zr,Ti)O_3$ (PZT) and barium titanate ($BaTiO_3$) have already been investigated to improve dielectric constant in a composite with organic polymers. The fibres in this thesis were doped with five types of piezoelectric ceramics, whose structural, microstructural, dielectric, hysteresis, resistivity, and pyroelectric properties seem promising.

1.3.1 BCZT

Barium calcium zirconate titanate ((Ba,Ca)(Zr,Ti)O_3, BCZT) is a lead-free piezoelectric material with excellent ferroelectric, dielectric and piezoelectric properties as well as large tunability [15]. Due to its excellent dielectric, ferroelectric and piezoelectric properties, this material is usable in a variety of applications, such as actuators, multilayer ceramic capacitors (MLCC), and positive temperature coefficient resistors (PTCR). However, this material requires a high sintering temperature (>1450 °C). In order to decrease the sintering temperature, it is necessary to produce powders with fine particle sizes and homogeneous distribution [16].

1.3.2 BT

Barium titanate ($BaTiO_3$ or BT) is an inorganic environmentally-safe ferroelectric material. It is chemically and mechanically stable and it demonstrate ferroelectric properties, high dielectric constant (ε_r) and low dissipation factor ($\tan\delta$) at and above room temperature [17]. It can be easily prepared and used in the form of ceramic polycrystalline samples. However, the preparation of is commonly involved with high temperature parameters or processes.. It is also known that the purity of the starting precursors affects the processing temperatures and hence the material properties [18]. Barium titanate composites are widely used in the fabrication of multilayer ceramic capacitors (MLC) and non-volatile memory devices [19].

1.3.3 KNN

Among the other lead-free ceramic materials, potassium sodium niobate, [(K,Na)NbO_3, KNN] is used in this research work because of its large piezoelectric response, ferroelectric properties and higher Curie temperature (>400°C). Potassium-sodium niobate is one of the most promising candidates because of relatively good comprehensive performance, low cost and lightweight [20]. The incorporation of KNN in the form of nanostructures also provides a unique connection between the higher aspect ratio nanostructured materials with very low loading [20].

1.3.4 TiO_2

Titanium dioxide (TiO_2) is a metal oxide semiconductor whose properties include non-toxicity, strong ultraviolet (UV) absorption, good stability and commonly energy band gap of 3.2 eV [21]. Titanium dioxide may be present in the rutile, anatase and brookite phases. The most commonly used, anatase phase, shows tetragonal crystalline structure, and is formed at temperatures around 450 °C [22]. TiO_2 occurs in many silicates in nature, accounting for over 1% of the earth's crust. Thus, it is manufactured using a variety of materials and processes [23].

1.3.5 ZnO

Zinc oxide (ZnO) received increasing attention from the scientific community in recent years [24]. The demand for ZnO is determined by a unique collection of properties that gives it an advantage over other materials in a number of parameters [25]. ZnO is a direct-band semiconductor with a band gap of 3.37 eV at 300 K and large exciton-binding energy (about 60 meV), which makes the exciton stable at room temperature. This material is characterized by high radiation stability - ZnO is able to work at high values of background radiation, for example, in space [24]. The enhanced interest is also connected with the wide application of ZnO in electronic and photonic devices and systems, including lasers in the blue and UV regions, UV LEDs and photodetectors, and nanostructures of numerous forms and purposes [26].

2. PREPARATION OF DOPED PVDF FIBRES

For the preparation of PVDF fibres doped with ceramics was used the method called **electrospinning**. Electrospinning is a simple method to produce nanoscale fibres both in a laboratory and industrially. Because of its wide application such as medicine, filtration [27], textile and other areas of industry, this technique has become one of the most acceptable methods for producing nanofibres. With this method, it is possible to reach nearly the theoretical limit of accuracy - the size of a molecule or atom [28]. Besides the polymer solution's intrinsic properties, the electrospinning processing conditions have a significant effect both on the β phase's proportion and the crystallinity of the electrospun PVDF [3]. 'In addition, the electrospinning process induces stretching in the fibrous web because of the application of the high electric field and in turn helps to transform α phase to β phase of the molecular chains in the crystals of PVDF.' [12, p. 2] In the last decade, research based on this method and its applications has increased, and this demonstrates the importance of electrospinning [28]. Some of the more active areas of application are composite fibres, carbon nanotubes, inorganic fibres, and tissue scaffolds.

The fabrication process starts with the application of a high electric field to the polymer or solvent solution. A Taylor cone is formed at the surface of the polymer solution extrusion, typically charged with high voltage (up to several tens of -kV), and it serves as the location of the ejection of an initial fibre [28]. Above a critical voltage, electrostatic repulsion overcomes the surface tension of polymer droplet developed at a needle tip attached to the syringe pump. Therefore, a charged polymer jet is ejected from the needle tip towards a grounded collector, leading to the formation of fibres [29]. Because of the chaotic trajectory of the polymer jet, the fibres collected on a grounded collector generally exhibit random orientation. The droplet is refilled by pumping new polymer solution to the needle tip through the needle. This is a widely used approach but is limited by needle clogging issues [30]. However, the needle can be easily unblocked with compressed air or by using a tool and unclogging the needle manually.

The prepared solutions were electrospun using the 4spin electrospinning equipment (Contipro a.s., Dolni Dobrouc, The Czech Republic). The collector (rotating metal drum covered by aluminium foil or Mylar® foil) is 20 cm far from the needle with an inner diameter of 1.067 mm (17 G). For the process was chosen PVDF a with molar mass of 275,000 g mol^{-1} (Sigma Aldrich, St. Louis, MO, USA). As solvents were used dimethylsulfoxide p.a. (DMSO, Sigma Aldrich, St. Louis, MO, USA) and acetone p.a. (Ac, Sigma Aldrich, St. Louis, MO, USA).

'The fibre diameter and porosity of the fibrous scaffolds depend on the processing parameters such as applied voltage, solution flow rate, type of solvent, polymer concentration in the solution, and the distance between the needle and collector.' [31, pp. 1-2] See table 2.1 for information parameters used to produce samples in this thesis. Resulting thickness of PVDF fibres is 1.5-0.3 μm. Properties of polymer solution also

result in a specific fibre morphology. SEM images of doped PVDF fibres created by the electrospinning method and used in this research can be found in the chapter 3.1 SEM images of samples.

Table 2.1 The electrospinning processing parameters for manufacturing PVDF fibres doped by piezoelectric ceramics

Material	**Additives**	**Cylinder speed [rpm]**	**Collector voltage [kV]**	**Collector distance [cm]**	**Spin time [min]**
PVDF	20% BT	300	50	20	100
PVDF	20% BCZT	300	50	20	100
PVDF	10% KNN	2000	50	20	30
PVDF	DMF+20% TiO2	2000	50	20	30
PVDF	20% ZnO	2000	50	20	30

2.1 Contipro 4SPIN LAB

The Contipro 4SPIN LAB is an electrospinning device used in the nanofibre production and the preparation of nanofibre layers from solutions of polymers (either biopolymers or synthetic polymers). It is a highly modular device constructed of specifically designed components. The emitters and collectors of 4SPIN are easily accessible as the 4SPIN device has a large transparent circular chamber without cables inside the chambre.

Selected process parameters are controlled by a central control system with a touch screen and multi-functional button. Key features of this instrument are real time monitoring of temperature and humidity, data logging to a PC, high voltage to 60 kV and multiple user logins option. ‘These additional settings of process parameters expand the opportunities for experimentation offered by the device.’ [32, p. 1]

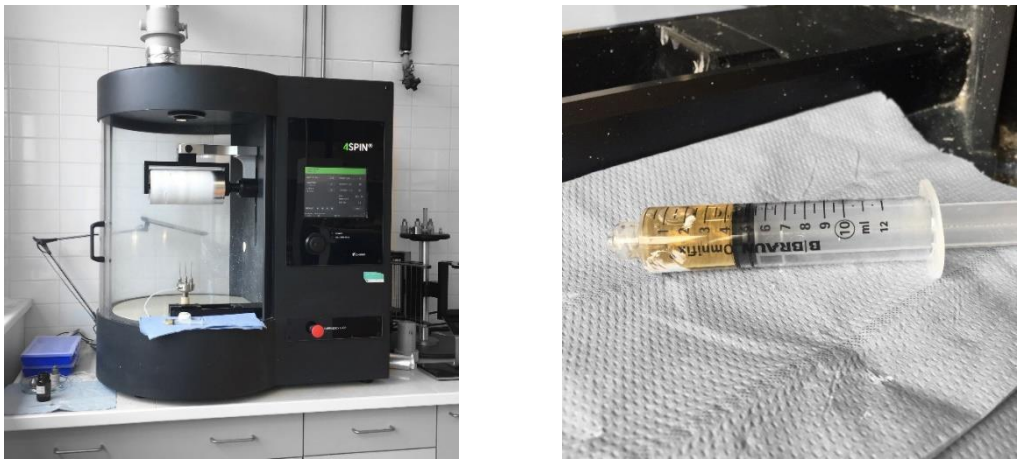

a) b)

Fig. 2.1 a) Electrospinning device Contipro 4SPIN LAB with needle emitter and rotating collector b) Polymer solution in a dispenser

3. Analysis of Doped PVDF Fibres

3.1 Scanning Electron Microscopy (SEM)

A SEM microscope is an electron microscope using a beam of focused electrons to scan a sample's surface; the process is based on applying kinetic energy to produce signals on the interaction of the electrons. An electron beam is emitted from so-called electron gun, is focused using electromagnetic lenses and travels as a stream of high-energy electrons towards a sample. Once the focused stream reaches the sample, it scans its surface in a rectangular raster. The interaction between the electrons and the sample causes emitting of secondary electrons, backscatter electrons, and X-rays. The scattered electrons are detected by a variety of detectors.

SEM analysis gives both insight into a sample's topography and can provide additional information about sample composition. The secondary electrons which are emitted from the specimen play the primary role of detecting the morphology and topography. Backscatter electrons are incidental electrons reflected backwards, and they show contrast in the composition of the elements of the specimen [33]. Although topographic information can be obtained using a backscatter detector, it is not as accurate as using secondary electrons. Diffracted backscatter electrons determine crystalline structures as well as the orientation of minerals and microfabrics. X-rays, emitted from beneath the sample surface, can provide quantitative elemental information [34]. Electrons reflected by the specimen are used to form a magnified, black, and white three-dimensional image.

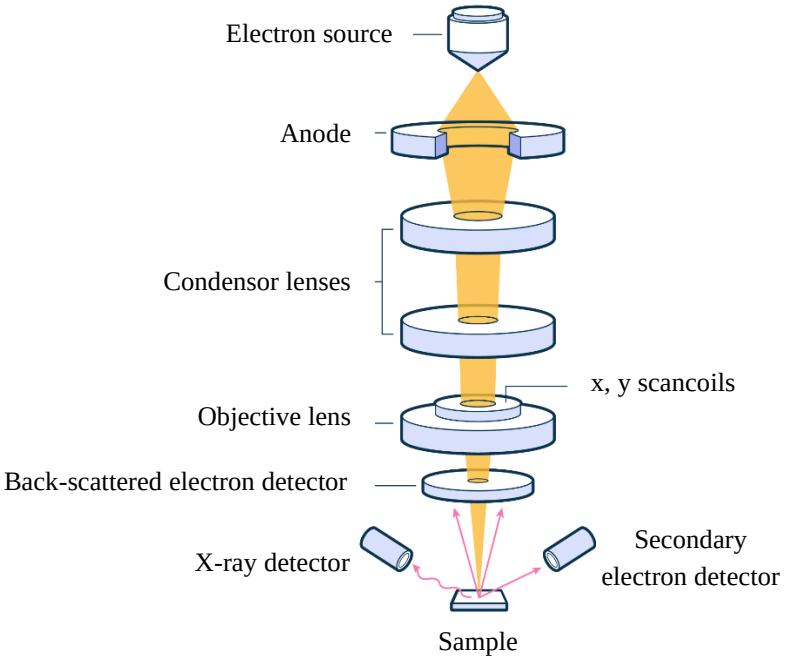

Fig. 3.1 Scanning electron microscope [33]

Despite the fact that SEM does not provide the resolution accuracy as transmission electron microscope (TEM), the intense interactions that take place on the surface of the specimen allows detailed surface characterization that includes a great depth of view and higher-resolution morphology scanning [35]. The advantages of a scanning electron microscope include its detailed three-dimensional and topographical imaging, versatile information garnered from different detectors as well as its wide array of applications. SEM has the potential to magnify an image up 10 nanometres [33], and the sample's size is limited only by the size of the electron microscope chamber. SEM microscopes are not complicated to operate, and associated software makes operation user friendly. When working with a scanning electron microscope, proper sample preparation plays an important role. While metals do not require complicated preparation, non-metals need to be coated with a conductive material to interact with electrons, see chapter 3.1.2 Sample preparation. Apart of that, most SEM samples require minimal other preparation actions. SEM devices work fast and often include SE, BSE and EDS analysers, similar to SEM microscope that was used to analyse our PVDF samples.

3.1.1 SEM microscope Tescan Lyra 3

Tescan Lyra 3 is a dual beam system with a versatile high-performance Ga ion source FIB, which is able to generate an image of the surface or to modify it with nanometric resolution (usually better than 10 nm) [35]. 'Focused ion beam scanning electron microscopes' (FIB-SEMs) implement a high-performance system including a high brightness Schottky emitter for achieving high resolution and low-noise imaging. The configuration in the FIB-SEM systems is set to coincide the electron and ion beam focal points [36].

Lyra 3 also includes Electron Dispersive X-Ray spectroscopy analyser (EDX) X-Max 50 from Oxford Instruments for elemental analysis, see chapter 3.2 Energy Dispersive Spectroscopy.

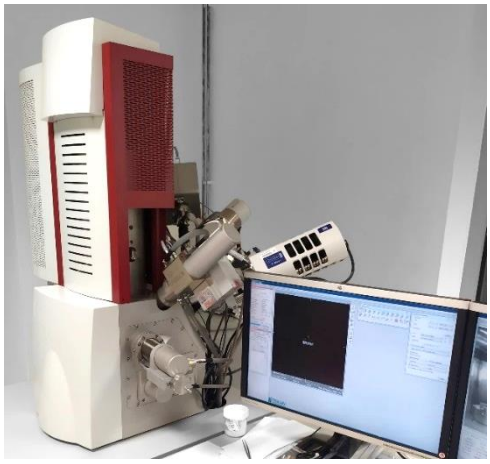

Fig. 3.2 Scanning electron microscope Tescan Lyra 3

3.1.2 Sample Preparation

SEM can image all kinds of samples: ceramics, metals and alloys, semiconductors, polymers, biological samples, and much more. However, the surface of the non-metal samples acts as an electron trap [33]. The resulting accumulation of electrons on the surface causes charging and influence the image information (creates white empty regions on the resulting image). When a metal coating is used, the conductive surface acts as a channel that allows the charging electrons to be removed from the material [37].

Polyvinylidene fluoride, as a non-metal, must be covered with a conductive material to allow observation in SEM. Creating a conductive layer of metal on the sample does not only reduces charging, but also reduces thermal damage and improves the secondary electron signal required for topographic examination in the SEM [38]. In this case, fine carbon and gold layers were used for analysed samples.

For the preparation of samples to be analysed with SEM was used a device Leica EM ACE600. It is a high vacuum film deposition instrument providing a deposition of ultra-thin coating of electrically conducting metal. Typically, it is equipped with Au sputter

target and carbon thread evaporation source; however, it is also possible to equip the device with other targets for sputtering. Processes are driven by built-in microprocessor control unit and a touch screen; protocols can be shared as the device supports a multi-user environment [39].

a) b)

Fig. 3.3 a) Coater Leica EM ACE600 b) Coated samples in holders

The coating technique used depends on the resolution and application. Typically, samples are mounted on a stub of metal with adhesive, coated with 10 - 20 nm of metal such as gold or palladium and then observed in the microscope. Historically, the most frequently used coating material has been **gold** because of its high conductivity and relatively small grain size, which makes it ideal for high-resolution imaging. The atoms of gold are sputtered from a ring-shaped target - when a high potential difference is established between electrodes, an electrical discharge passes between them. The cathode electrode is then bombarded by positive ions of a residual gas such as argon. This bombardment results in atoms of the cathode material (gold) being sputtered off and transferred to nearby surfaces, upon which the atoms impinge from statistically random directions [40].

If energy-dispersive X-ray (EDX) analysis is required, SEM users typically coat their samples with **carbon** due to the fact that carbon's X-ray peak does not conflict with the peak of any other element [37]. A carbon source can be either in the form of a thread or rod; in this case, it was a carbon thread, see Fig. 4.2 a). The source is mounted in a vacuum system between two high-current electrical terminals. When the carbon source is heated to its evaporation temperature, a fine stream of carbon is deposited onto specimens using the same procedure as described above for gold [40]. This process removes a considerable amount of carbon particles – in Fig. 3.4 a) is visible that the carbon thread was so fragile after the deposition that it tore. After each coating, it is necessary to exchange the carbon thread for a new one, see Fig. 3.4 b). Other coating materials include tungsten, iridium, chromium, platinum, palladium, or silver [37]. It is essential to use clean laboratory

tweezers, forceps and gloves while handling the samples, as well as to store the samples in a dry, clean environment.

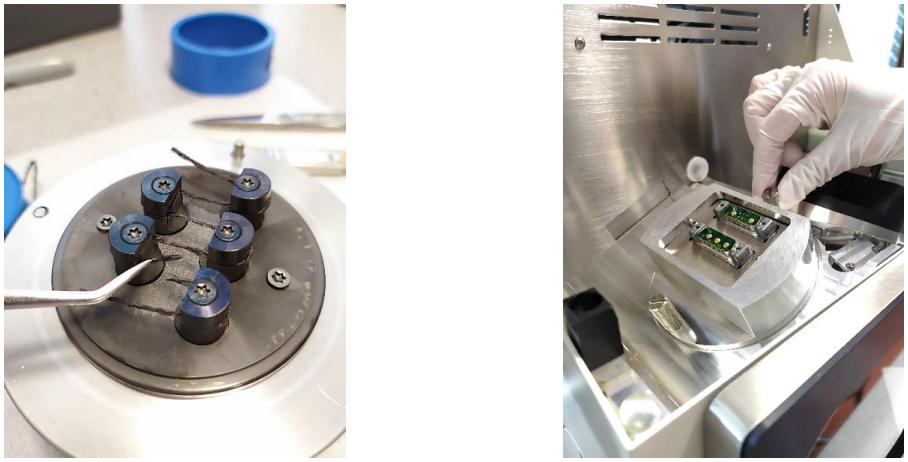

a) b)

Fig. 3.4 Coater Leica EM ACE600 a) Carbon thread aperture b) Changing of carbon thread

3.1.3 SEM images of samples

The following micrographs show fibre morphology and diameter distributions obtained by electrospinning of PVDF. The fibres have an inhomogeneous diameter; the thin fibres are predominantly smooth, while the wider fibres have a rough texture with a layered structure. It can be observed that ceramic particles are uniformly dispersed throughout the polymer with little agglomeration in some localized regions. It suggests that the ceramic particles have been incorporated into the fibres; however, to support this argument, EDX analysis must be performed.

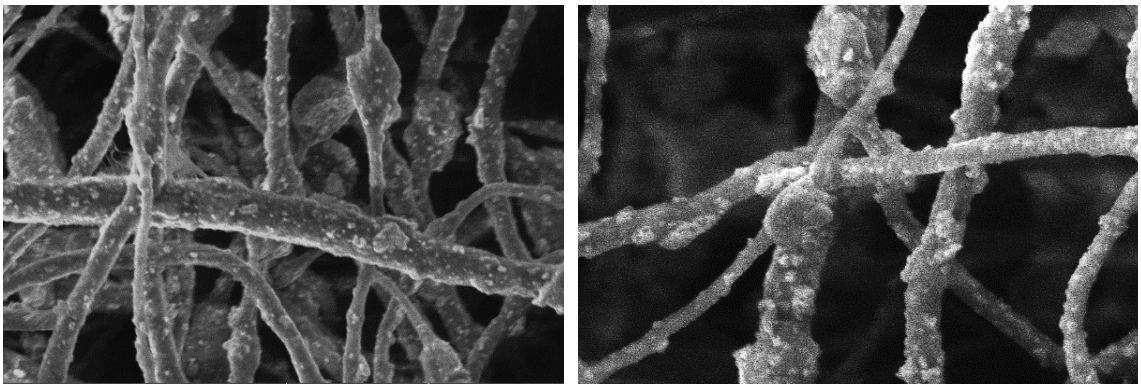

a) b)

Fig. 3.5 Sem micrograph of PVDF/BCZT composite with a field view a) 20µm b) 10µm

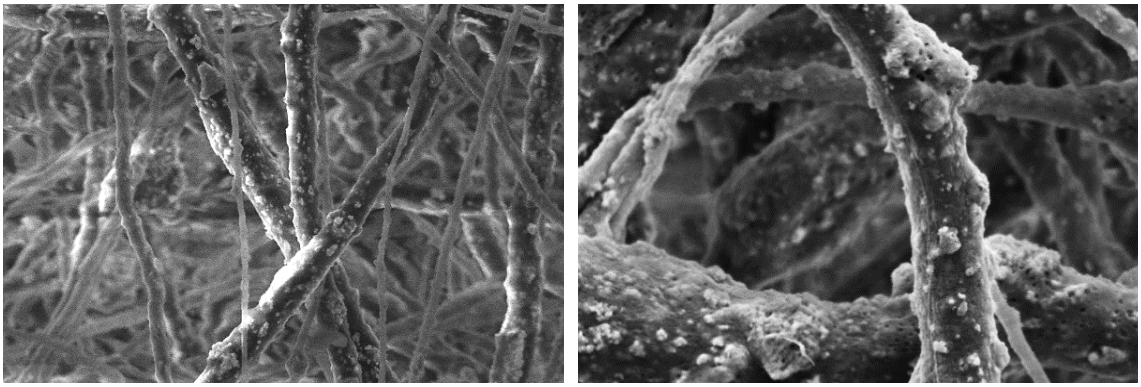

a) b)

Fig. 3.6 Sem micrograph of PVDF/BT composite with field view
a) 20µm b) 10µm

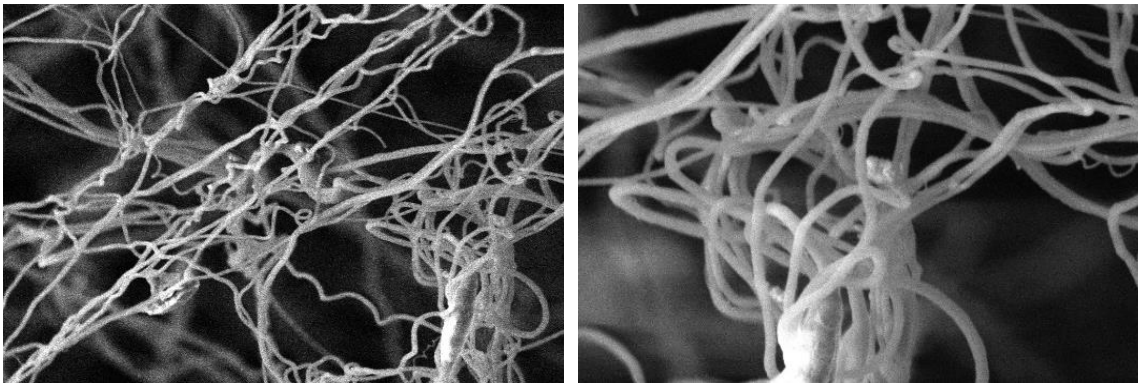

a) b)

Fig. 3.7 Sem micrograph of PVDF/KNN composite with field view
a) 20µm b) 10µm

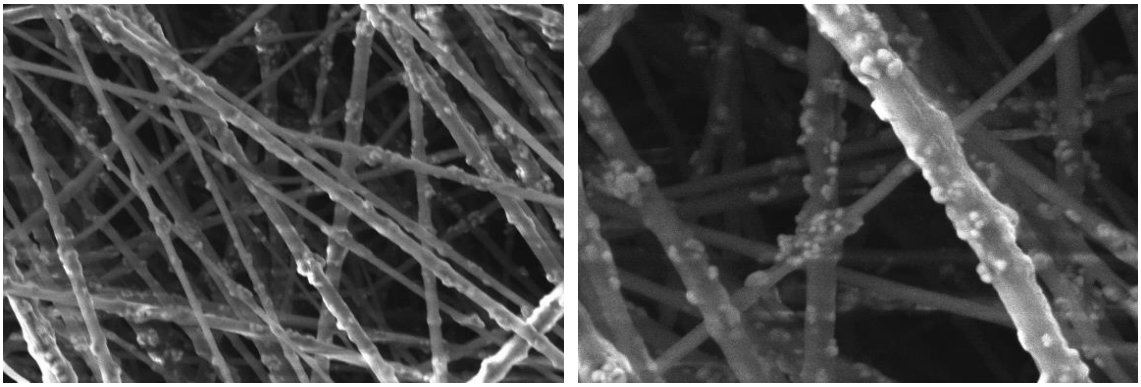

a) b)

Fig. 3.8 Sem micrograph of PVDF/TiO_2 composite with field view
a) 20µm b) 10µm

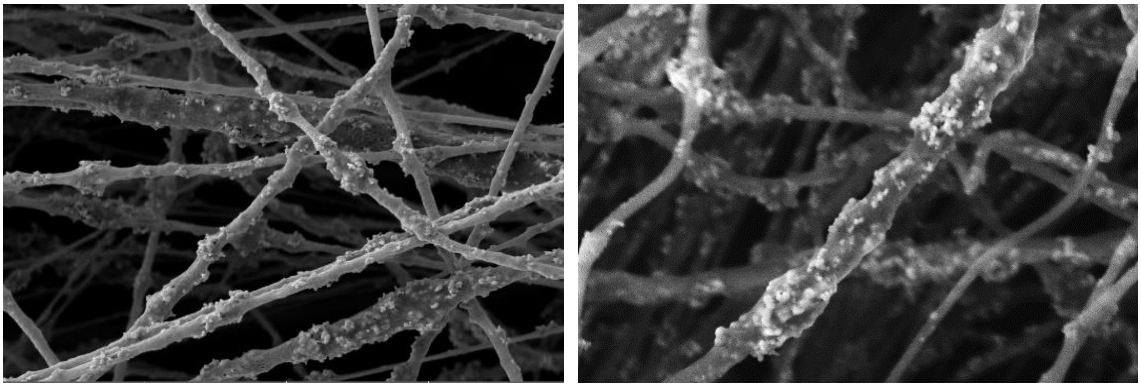

a) b)

Fig. 3.9 Sem micrograph of PVDF/ZnO composite with field view a) 20μm b) 10μm

3.2 Energy Dispersive X-ray Spectroscopy (EDX)

Energy-dispersive X-ray spectroscopy (EDS) is a standard method for the elemental analysis or chemical characterization of a very small sample of material (even a few cubic micrometres). A properly equipped SEM microscope, similar to SEM microscope used for analysis of doped PVDF in this thesis, often contains the instrumentation to perform EDX analysis, as the technology required to generate a high energy beam of charged particles (for example electrons) is already present. The SE detector makes it possible to monitor the morphology (shapes and sizes with defined resolution), while the EDX detector allows the microelement analysis of the samples (elemental analysis with defined resolution).

As explained in Encyclopedia of Interfacial Chemistry published by Elsevier, 'its characterization capabilities are due in large part to the fundamental principle that each element has a unique atomic structure allowing a unique set of peaks on its X-ray spectrum' [41, p. p. 322]. A high-energy beam of charged particles (such as electrons or protons), or an X-ray beam, is directed into the studied sample to stimulate the emission of characteristic X-rays from the sample. Being excited by this beam, the X-rays emitting from the sample are characteristic of the atomic structure of the elements and allow the identification of the elements by comparison with reference spectra.

The X-ray emissions can be analysed using an energy-dispersive detector, a solid-state device that discriminates among X-ray energies. 'Appropriate elements are assigned, yielding the composition of the atoms on the specimen surface.' [42, p. 49] The number and energy of the X-rays emitted from a specimen can be measured by an energy-dispersive spectrometer. The energy of the X-rays (difference in energy between the shells) is characteristic of the atomic structure of the element from which they were emitted. It is, therefore, possible to identify the composition of the sample.

3.2.1 EDX micrographs of Samples

Besides the ability to investigate the sample surface, the Lyra 3 FIB-SEM allow attaching many other detectors and accessories to the chamber from the outside – for example EDX detector. This approach is valuable and timesaving, as the technology required to generate a high energy beam of charged particles (for example electrons) is already present, and it is possible to perform SEM analysis together with EDX analysis. Images below were created using this approach. The distribution of individual particles in the fibres is visible, distinguished by colours.

The presence of ceramic particles in the fibres were confirmed by mapping using energy dispersive spectroscopy (EDX mapping, Tescan Lyra 3, AZtec software). The measurement was performed at an accelerating voltage of 10 kV and energies of 0–10 keV were measured. The aim was to create as homogenous composite as possible, where properties are uniform throughout the fibre, i.e., they do not depend on the position inside the fibre body.

Figures 3.10 – 3.14 present map analysis of the major elements; these elements are colour-coded by EDX software. It is visible that the added ceramics relatively homogeneously copies the structure of PVDF nanofibres, which means that the additive is homogeneously dispersed in the polymer fibres formed by electrospinning; thus, the desired result was obtained.

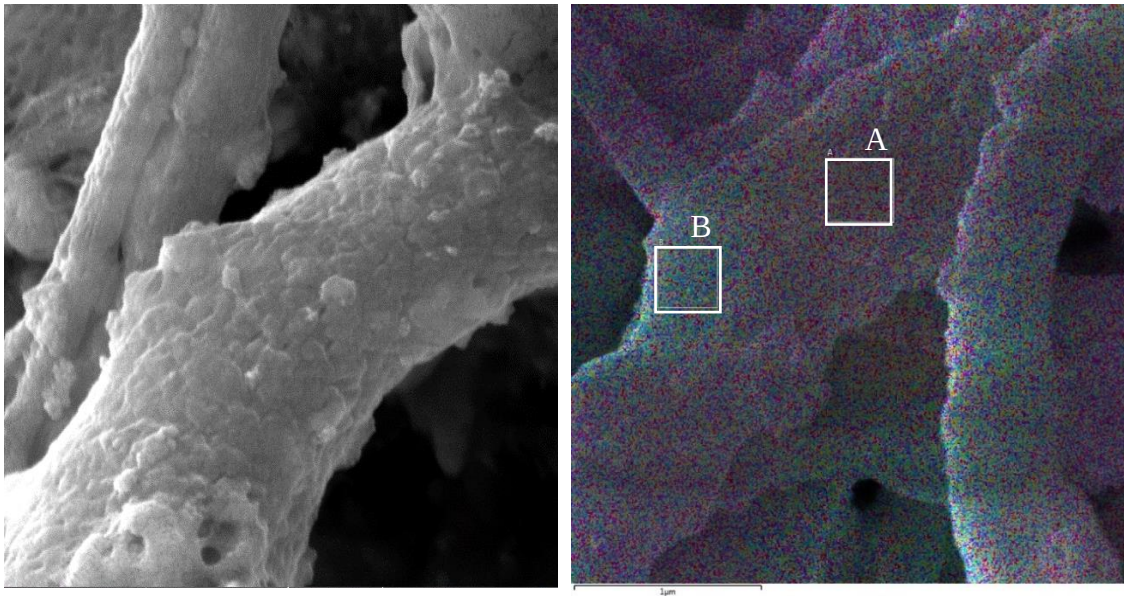

a) b)

Fig. 3.10 PVDF/BCZT composite with field view 3 μm
a) SEM micrograph b) EDX micrograph

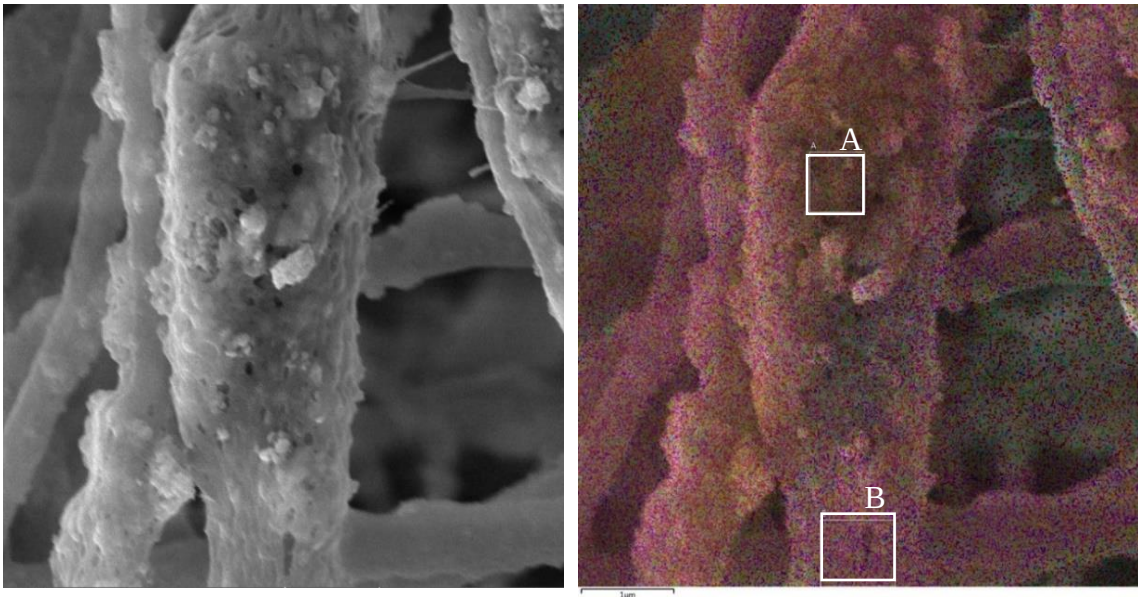

a) b)

Fig. 3.11 PVDF/BT composite with field view 6 µm
a) SEM micrograph b) EDX micrograph

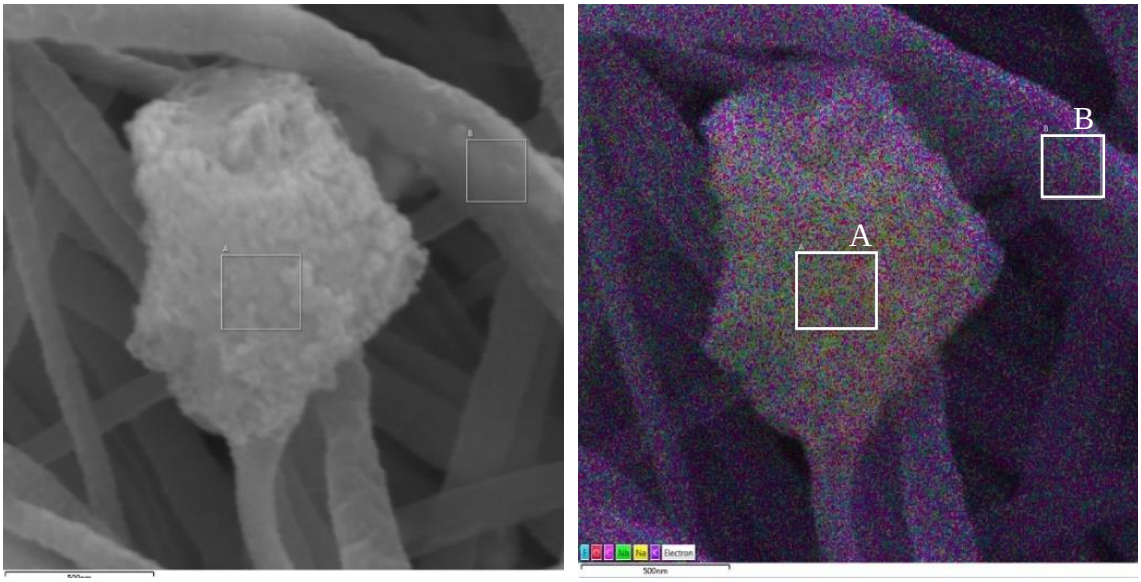

a) b)

Fig. 3.12 PVDF/KNN composite with field view 2 µm
a) SEM micrograph b) EDX micrograph

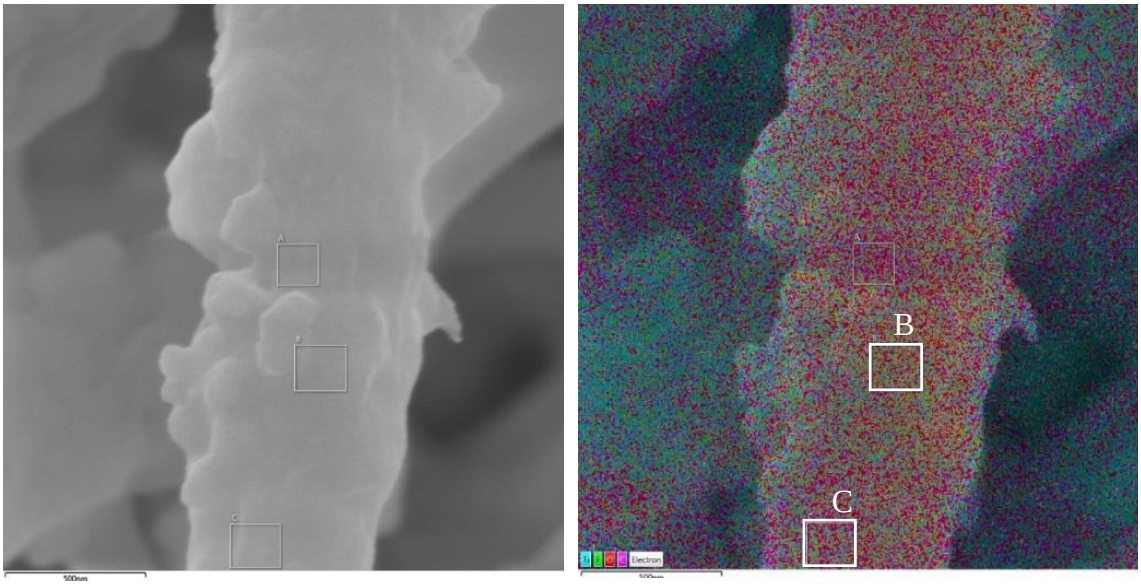

a) b)

Fig. 3.13 PVDF/TiO_2 composite with field view 2 µm
a) SEM micrograph b) EDX micrograph

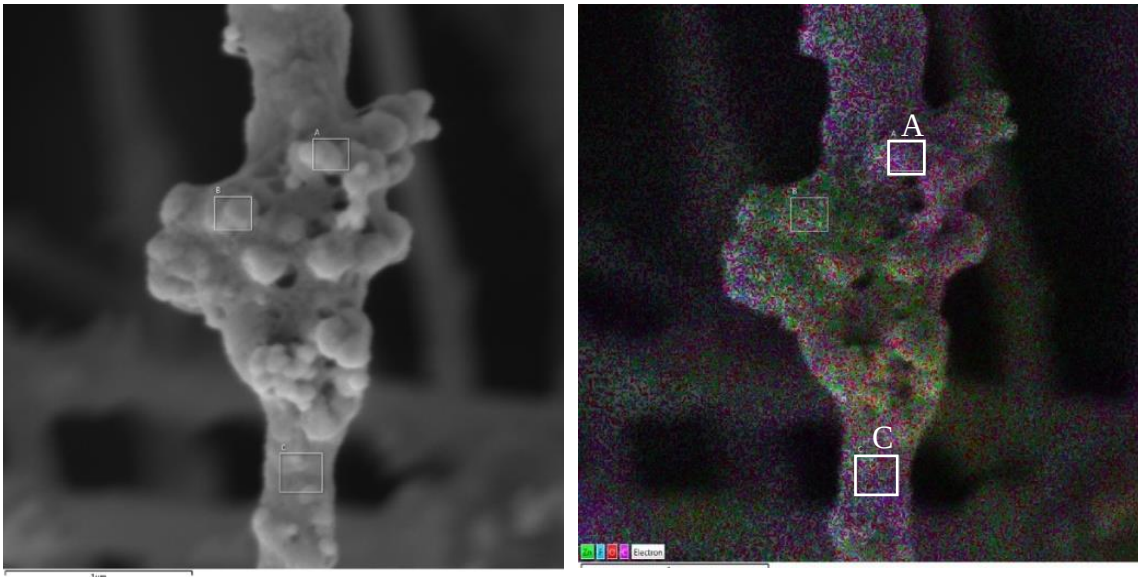

a) b)

Fig. 3.14 PVDF/ZnO composite with field view 3 µm
a) SEM micrograph b) EDX micrograph

EDX analysis also presents a spectrum that plots the number of X-rays detected versus their energies. In other words, it displays the peaks correlated to the elemental composition of the investigated sample and allows the identification of elements present in the sample. Using the AZ software, it is also possible to concentrate only on a specific fibre section. This feature is ideal for comparing elemental compositions of various fibres areas - see highlighted sections in EDX micrographs. These sections are further investigated in following figures.

See also the atomic percentage of each section in the upper right corner of each graph. These reveal the atomic composition of each area, not influenced by the weight of each element. Only a slight difference in atomic percentages of elements in each section's composition supports the previous arguments. It can be concluded that fibres have been doped successfully with even distribution.

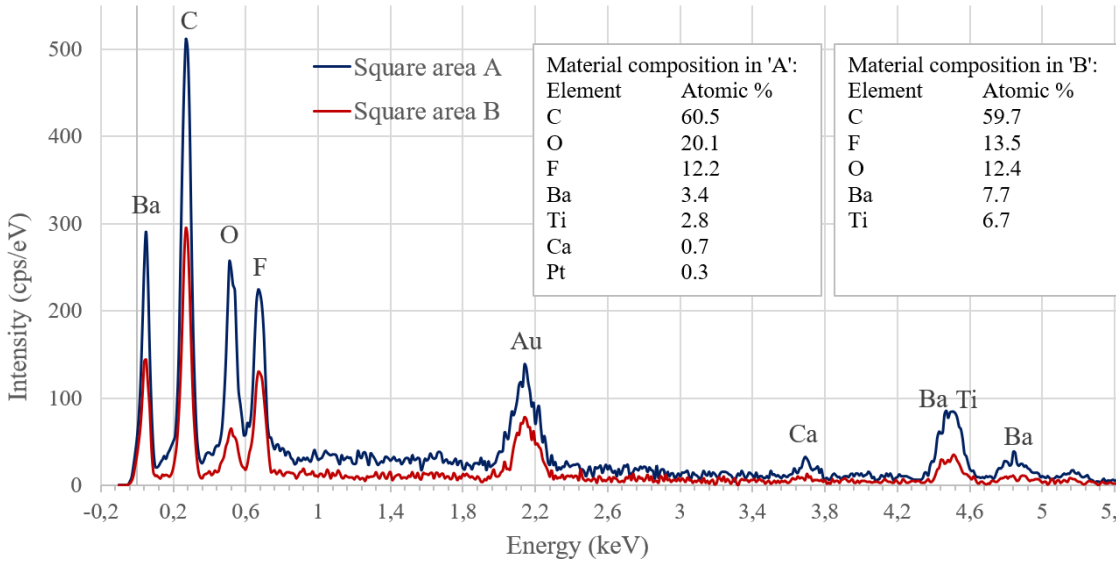

Fig. 3.15 EDX spectrum of PVDF fibres doped by BCZT

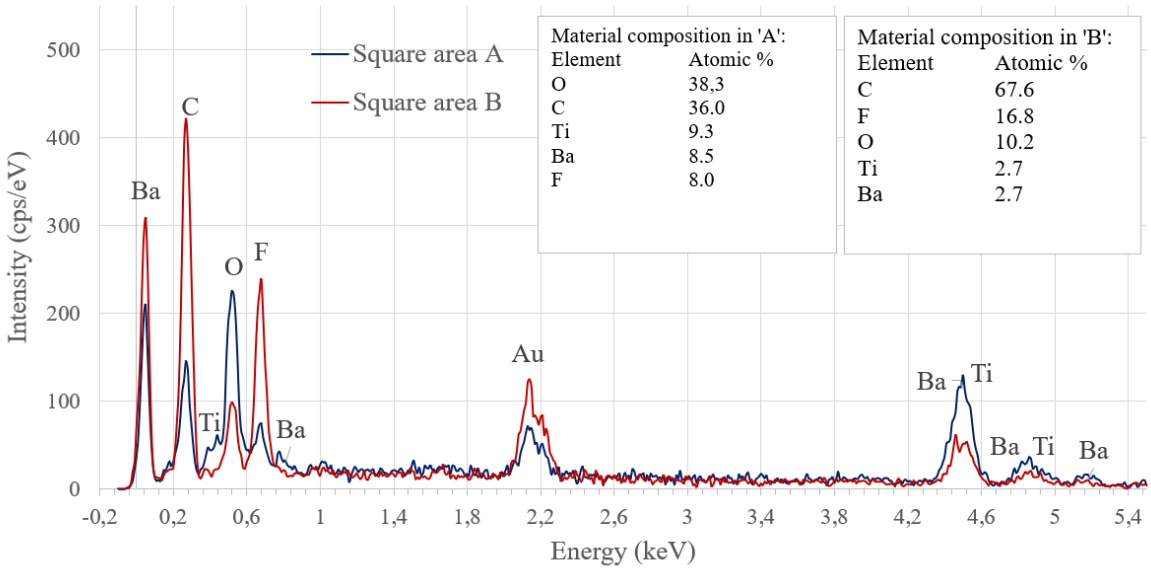

Fig. 3.16 EDX spectrum of PVDF fibres doped by BT

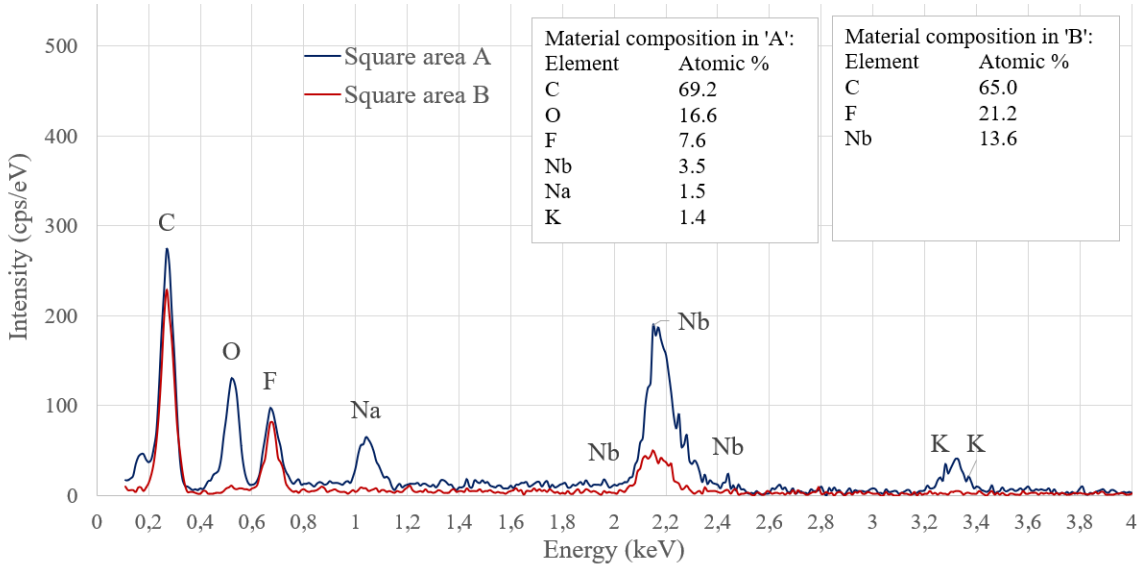

Fig. 3.17 EDX spectrum of PVDF fibres doped by KNN

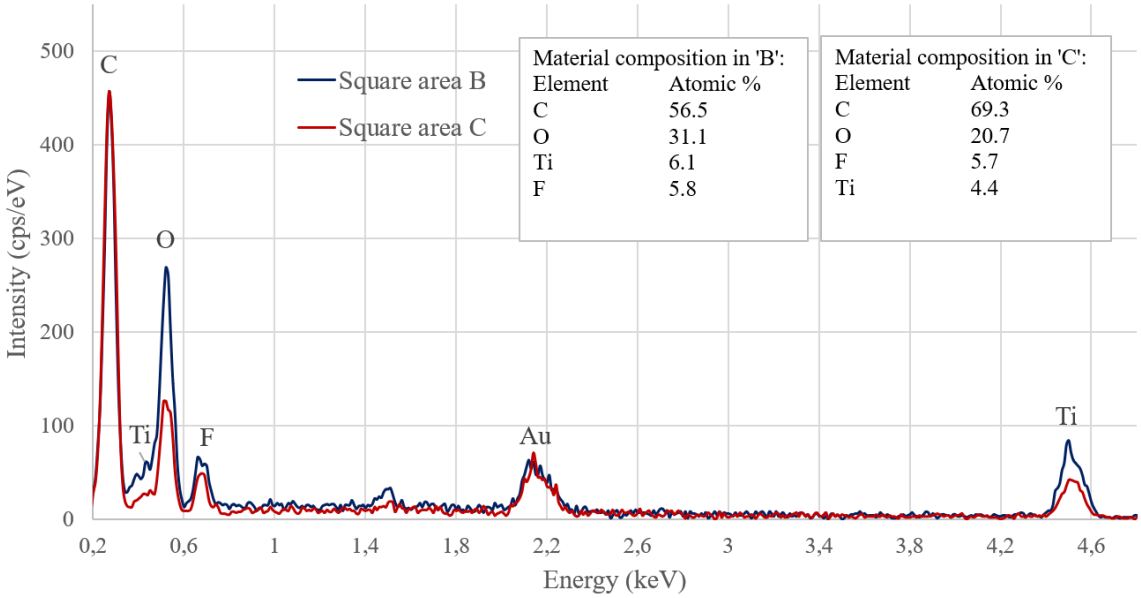

Fig. 3.18 EDX spectrum of PVDF fibres doped by TiO_2

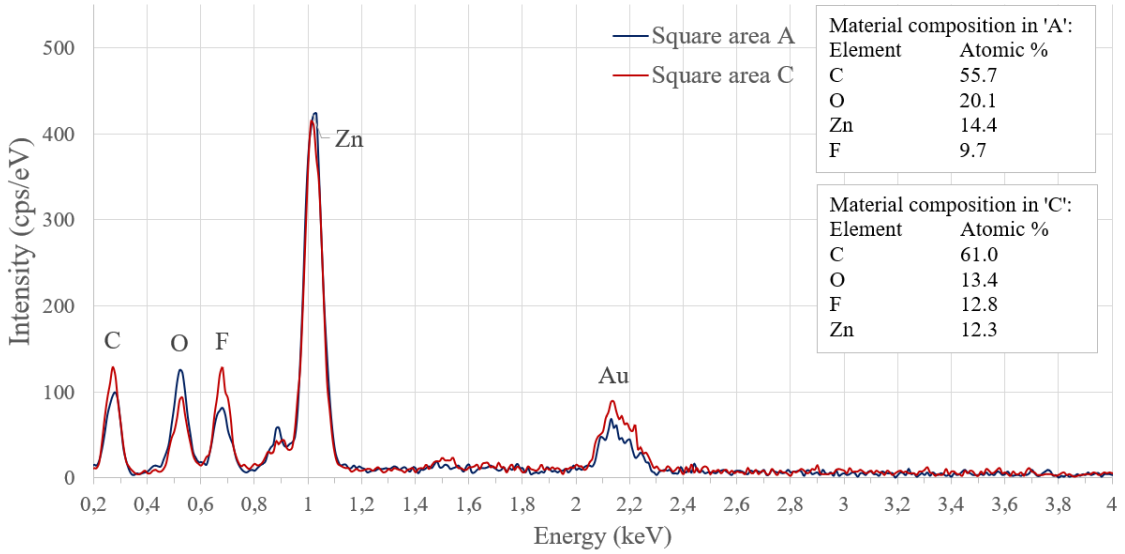

Fig. 3.19 EDX spectrum of PVDF fibres doped by ZnO

3.3 Fourier Transform Infrared Spectroscopy (FTIR)

Vibrational spectroscopy embraces a range of techniques that detects molecular vibrations in samples. Generally, these techniques include Raman and Infrared spectroscopy, which are complementary techniques resulting from changes in vibration modes of molecules [43]. FTIR spectroscopy is based on the interaction of IR radiation and natural vibrations of the chemical bonds among atoms. Vibration modes which result in changes in the dipole moment of a module are IR active, and those that result in changes in polarizability are Raman active [44].

With this technique, it is possible to detect all transmitted energy simultaneously by application of interferometer and fast Fourier transform algorithm. The principle of FTIR spectroscopy is based on irradiating the sample with IR radiation and detecting changes in the absorption of the radiation. Sample molecules are exposed to infrared radiation and absorb radiation of specific wavelengths. This action causes a change of dipole moment of these molecules and a transfer of vibrational energy levels from the ground state to an excited state in these molecules. As the vibrational motion changes (either by changing the bond length or bond angle), it causes the formulation of absorption bands in the vibrational spectrum. By analysing the spectrum, it is possible to obtain structural information of a molecule, as the intensity of absorption peaks is related to the change of dipole moment and the possibility of the transition of energy levels. Molecular vibrations can range from the simple coupled motion of the two atoms of a diatomic molecule to the much more complex motion of each atom in a large polyfunctional molecule [45].

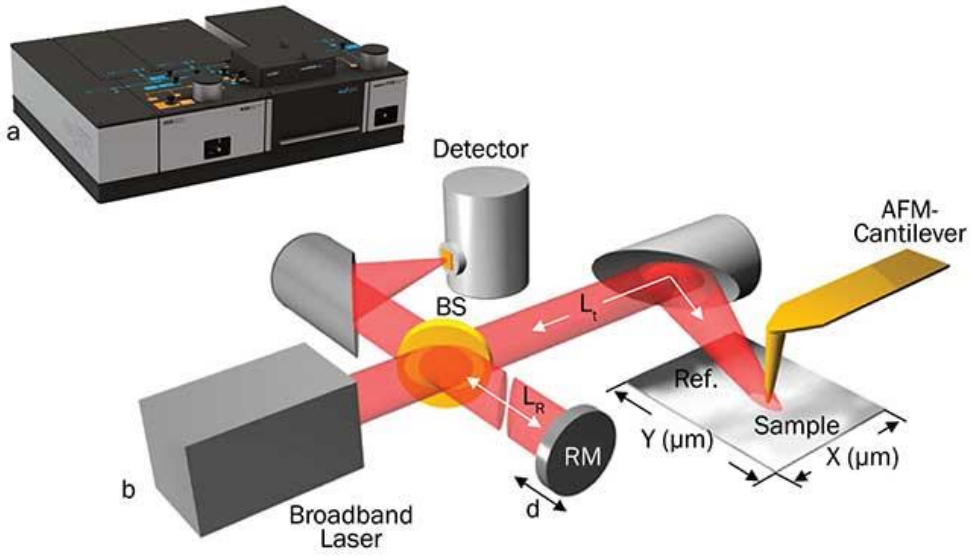

Fig. 3.20 Schematic diagram depicting the optical components of the FTIR system similar to the system used in this thesis but enriched for AFM-Cantilever. [46]

3.3.1 Device for FTIR analysis VERTEX 70v

FTIR analysis was performed on Vertex 70 V (Bruker, Billerica, MA, USA), set up by accumulating 512 scans with a resolution of 1 cm^{-1} in transmission mode. 'The data acquisition is based on two-channel delta-sigma ADCs with 24-bit dynamic range, which is running in parallel and integrated into the detector preamplifier electronics.' [47, p. 1] With this device, it is possible to obtain results in the scale of sub-monolayers without weak spectral features caused by water vapour or CO_2 absorptions. VERTEX is also suitable for suppressing external signals, automatic set up, recognition of sampling accessories and optical components and check of measurement parameters [47].

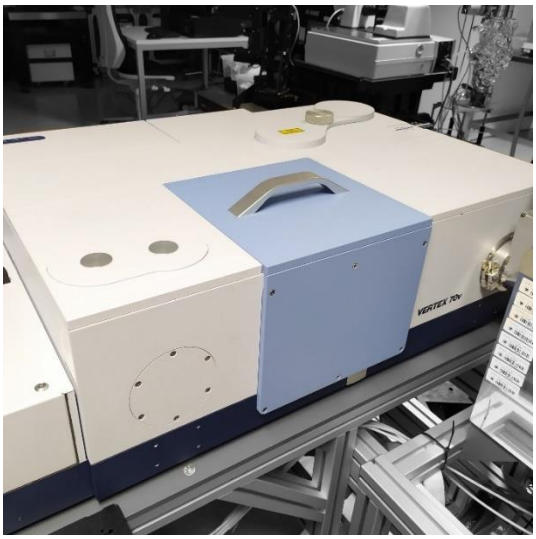

Fig. 3.21 FTIR spectroscope VERTEX 70v

3.3.2 FTIR analysis of samples

The effect of nanostructures in the nanocomposite materials is further authenticated by FTIR analysis. Following figures show the FTIR absorbance spectra of PVDF nanocomposite fibres in the 400-1600 cm^{-1} region. Most of the vibrations are coupled below 1500 cm^{-1} because majority of the single bonds are absorbed at single frequency [48].

The FTIR spectra of PVDF-BCZT nanocomposite fibres are depicted in Fig. 3.22. The spectrum shows characteristic FTIR bands corresponding to nanocomposites' constituents, indicating the significant interaction between them.

The characteristic band from the electroactive β,γ-phase is clearly visible at 838 cm^{-1} [3]. Some of characteristic bands of crystalline α-phase have been observed at 759 and 975 cm^{-1} and the band at 1275 cm^{-1} exists due to β crystalline phase of PVDF [48] [49]. The shifts of FTIR peaks in the nanocomposite infer the existence of some interaction between the polymer matrix and the fillers [50].

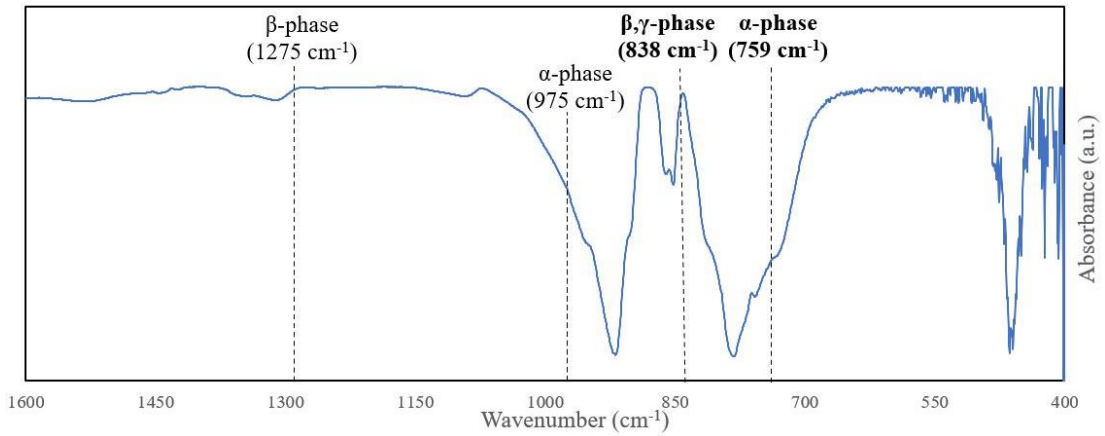

Fig. 3.22 FTIR spectrum of PVDF fibres doped by BCZT

The FTIR spectrum in Fig. 3.23 shows that the spectrum of the next sample (PVDF-BT) has the same peak position but different intensity.

Characteristic bands from the β-phase have been identified at 510 and 1275 cm^{-1} and characteristic bands of crystalline alpha-phase have been observed at 615 cm^{-1}, 758 cm^{-1} and 975 cm^{-1}. The peak observed at 840 cm^{-1} belongs to β,γ phase [48] [49].

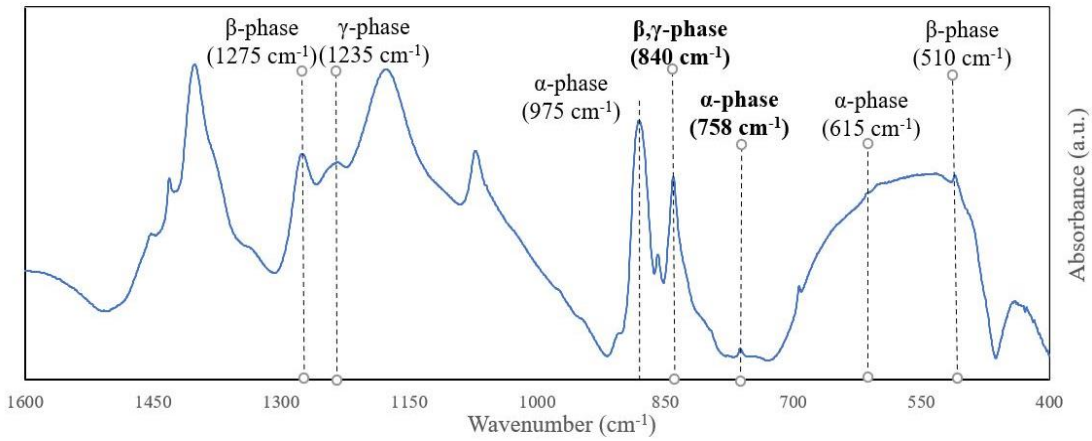

Fig. 3.23 FTIR spectrum of PVDF fibres doped by BT

The effect of KNN nanostructures in the nanocomposite materials is shown in Fig. 3.24. The peak of crystalline β,γ phase is evident at 840 cm-1 similar to peaks of γ at 1235 cm-1 and α at 615 $cm^{-1,}$ 760 cm^{-1} and 975 cm^{-1} [3]. Characteristic features of the β phase with peaks at 510 cm^{-1} and 1270 cm^{-1} are clearly visible as well [48] [49].

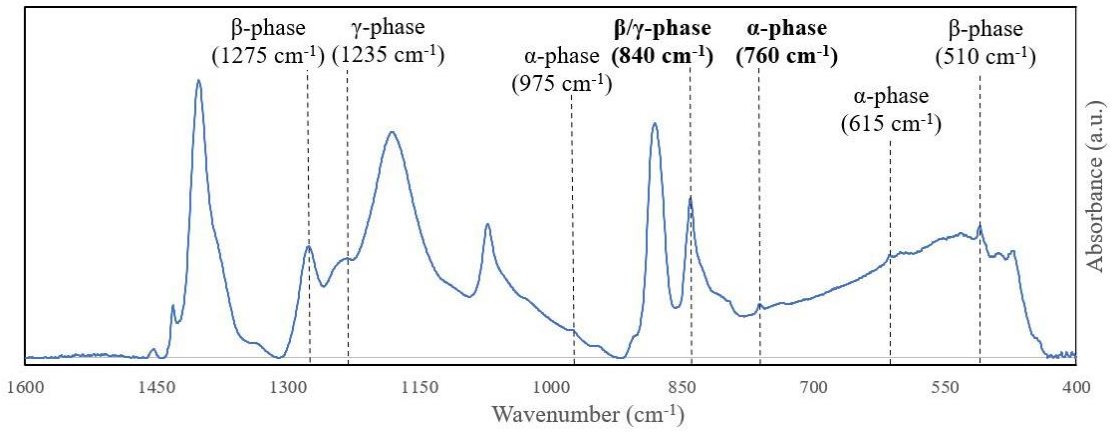

Fig. 3.24 FTIR spectrum of PVDF fibres doped by KNN

The FTIR spectra of PVDF-TiO2 nanocomposite fibres are depicted in Fig. 3.25.

Band of the electroactive β,γ phase have been identified at 840 cm^{-1}, and features of β crystalline phase are visible at 510 cm^{-1} and 1270 cm^{-1}. The peaks of α are low, but can be observed at 615 cm^{-1}, 760 cm^{-1} and 975 cm^{-1} [48] [49].

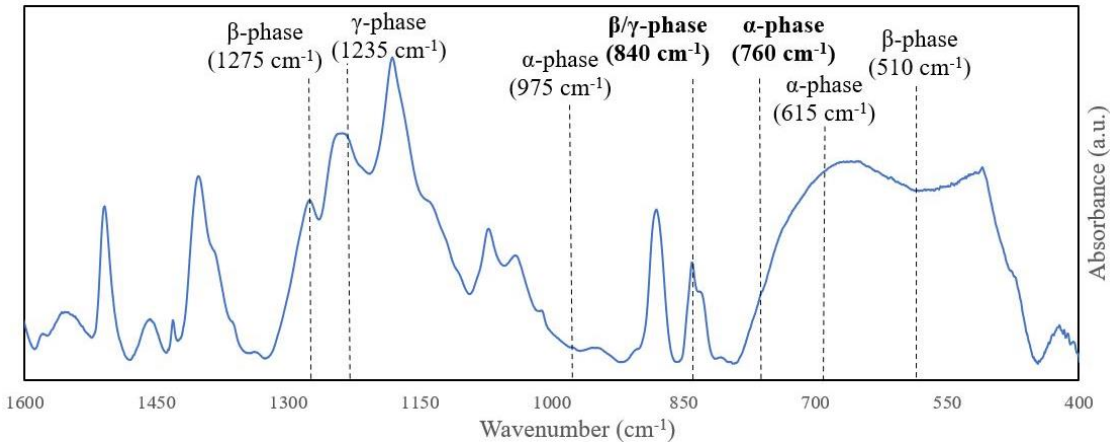

Fig. 3.25 FTIR spectrum of PVDF fibres doped by TiO_2

The FTIR spectrum of the nanofibre of PVDF-ZnO nanocomposite fibres demonstrates vibration peaks at 512 and 1275 cm^{-1}, which are typical vibration characteristics of the β crystalline phase according to the previous research and findings [48] [49]. Characteristic band of crystalline α-phase have been observed at 760 cm^{-1}, the characteristic band of crystalline γ-phase at 1235 cm^{-1} and the peak at 840 cm^{-1} belongs to β,γ phase [3] [51].

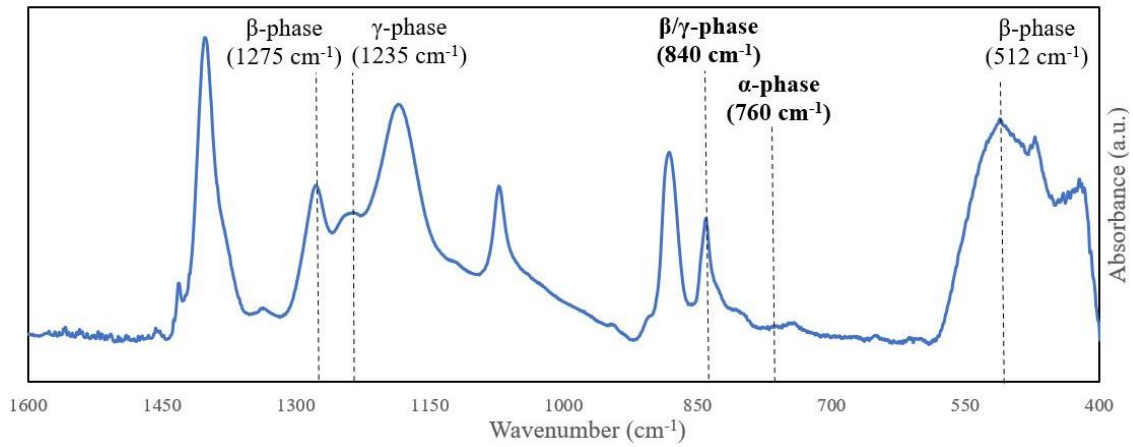

Fig. 3.26 FTIR spectrum of PVDF fibres doped by ZnO

In all analysed PVDF nanocomposites, the peaks associated with α-phase were significantly reduced with concurrent increased in the β-phase. The spectra of nanocomposites clearly suggest the successful formation of new PVDF nanocomposites due to significant interaction between ceramics and polymer chain (possessing the properties of both components). It can be concluded that the nanofillers modify the phase structure of the PVDF and convert it to the pure β-γ phase, which of course, would potentially be responsible for the enhanced piezoelectric property. Therefore, it can be concluded that nanocomposites have been prepared successfully.

To determine the relative fraction of the β and γ phase (F_{ea}) in each sample, the absorbance differences of α and β,γ phases and are evaluated [51]. The α and β,γ phases are measured at wavelengths ≈ 763 cm^{-1} and ≈ 840 cm^{-1}. Phase composition should be chosen according to practical application.

Table 3.1 Fourier Transform Infrared Spectroscopy (FTIR) phase calculation

	BCZT	**BT**	**KNN**	**TiO_2**	**ZnO**
Relative fraction of the β and γ phases (F_{ea})	93,37	97,87	63,92	96,75	87,37

3.4 Raman spectroscopy

Raman spectroscopy is a fast and non-destructive instrumental method that can be used to identify and compare chemical compounds. The method uses the so-called Raman effect, an inelastic scattering of monochromatic radiation on material particles, which occurs when the laser beam interacts with the atoms of the investigated material. The Raman effect describes the shift in wavelength of scattered radiation of examined sample from excitation radiation (from a source of monochromatic radiation). Since each substance shows a characteristic wavelength shift, this phenomenon can be used to identify the chemical composition of a sample of material of different states, determine the number of elements represented or analyse the structure. The Raman spectrum presents chemical composition information; the characteristic peaks (or bands) are directly related to the vibration state of the chemical bonds [52].

Raman imaging systems combine an ultrahigh-throughput spectrometer system (UHTS) with a sensitive confocal microscope. The laser beam is focused on the sample, and the Raman signal is collected again via the same optical path. The Raman effect is extremely weak, hence every Raman photon is essential for imaging [53]. The precise adjustment of all optical and mechanical elements allows the detection of Raman signals of even weak Raman scatterers and minimal material concentrations or volumes with the lowest excitation energy levels. Raman spectroscopy is non-destructive and does not require any specific sample preparation. ‘The sample can be measured directly in glass container or in case of pharmaceuticals samples can be measured in original sachets.’ [54, p. 1]

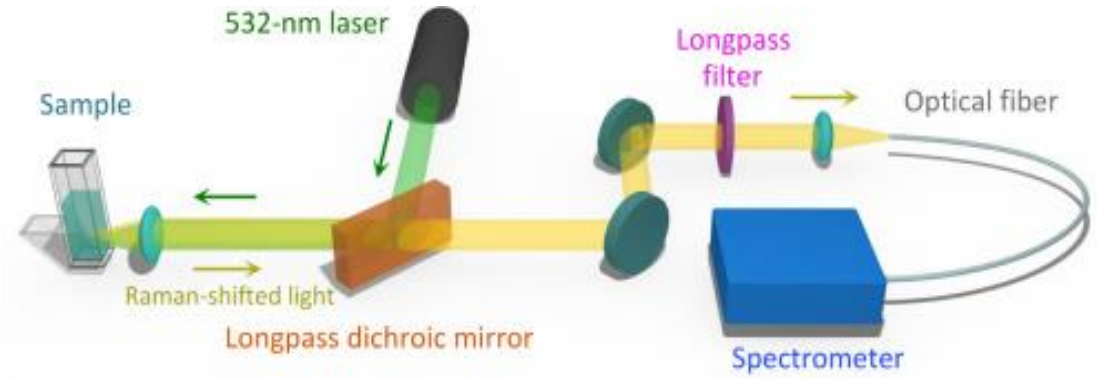

Fig. 3.27 The experimental scheme for the Raman-spectroscopy-based concentration sensor (RCS) [55]

Laser sources for Raman spectroscopy vary in wavelengths from the near-UV to the near-IR (NIR) range. ‘A monochromatic light beam of high intensity laser can be used in UV, visible or IR regions in Raman measurements whereas in IR spectroscopy the range is limited to IR frequencies.’ [54, p. 1] One of the significant drawbacks of Raman spectroscopy is that the sample may show fluorescence emission that causes saturation of the CCD detector after being excited with laser light. However, fluorescence can be overcome by using different laser sources; it is beneficial to have a Raman instrument equipped with at least three different lasers. The most widely used laser sources emit at 532 (green), 633 (red), and 785 nm (NIR), or comparable wavelengths. The most appropriate laser source for PVDF doped with piezoelectric particles is the green laser source [56].

3.4.1 Raman Microscope Alpha300 R

The Alpha300 R is a confocal Raman microscopy system with laser wavelength from UV to NIR. ‘It allows hyperspectral image generation with the information of complete Raman spectrum at every image pixel with a resolution down to the optical diffraction limit.’ [57, p. 1] Key features of this instrument are several configurations with different features to fulfil a wide variety of customer requirements, true confocality, ideally suited to depth profiling and 3D Raman image generation and throughput optimized UHTS spectrometers with a variety of focal lengths. Alpha300 R also includes Fast Raman Imaging and Ultrafast Raman Imaging with motorized or piezo-driven scanning stages for time-saving high-quality measurements [57].

Fig. 3.28 Raman Microscope Alpha300 R

3.4.2 Raman analysis of samples

The following figures show the Raman spectra of PVDF nanocomposite fibres. Raman was measured using 5mW laser power, and for spectra acquisition was used 532 nm laser. The exposition time was set at 10 sec, and the number of accumulations was 20. The Raman spectra provide additional data about the skeleton chain, but the β,γ phase peak is in some spectra hard to distinguish (at ≈ 840 cm^{-1}). Some powders undergo structural changes when incorporated into the polymer, causing peaks to have a different peak height ratio than pure powder. The evident peak of PVDF/ZnO nanocomposite indicates enhanced performance compared to other samples and could result in higher permittivity. See next chapter for permittivity measurement.

These features appear with a strong luminescence background, so it is difficult to comment on the Raman data changes in α- and β-phases from the Raman data. One possible explanation of this occurrence may be the possible conversion of a part of the α-phase into the β-phase, as confirmed by FTIR spectra.

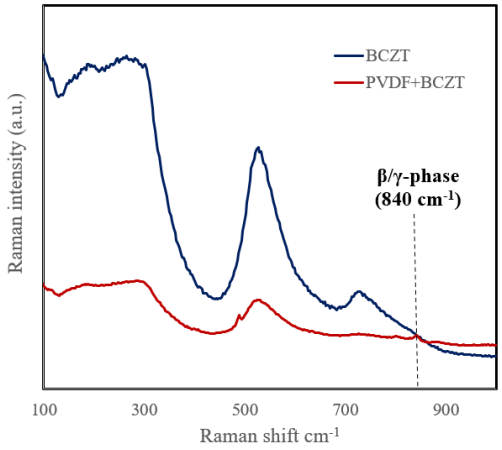

Fig. 3.29 Raman spectra of PVDF doped by barium calcium zirconate titanate (BCZT)

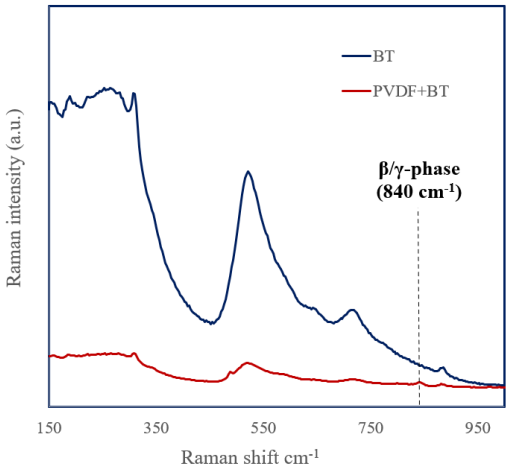

Fig. 3.30 Raman spectra of PVDF doped by barium titanate (BT)

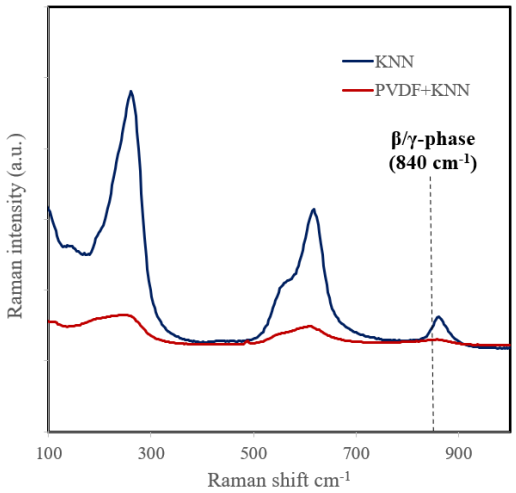

Fig. 3.31 Raman spectra of PVDF doped by potassium sodium niobate (KNN)

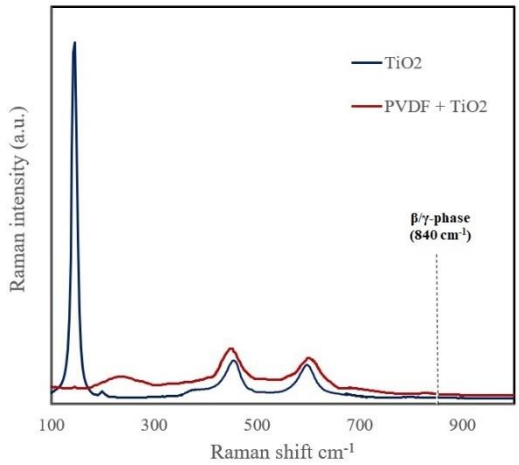

Fig. 3.32 Raman spectra of PVDF doped by titanium dioxide (TiO_2)

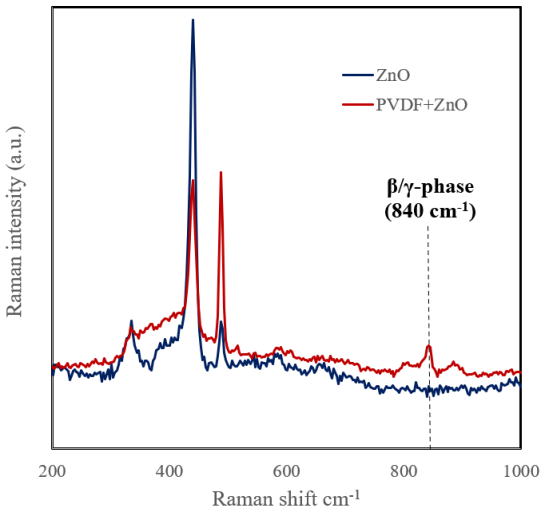

Fig. 3.33 Raman spectra of PVDF doped by zinc oxide (ZnO)

3.5 Measuring of dielectric constant

The dielectric constant defines the polarisation ability of the material. It was reported that the dielectric properties of composite material are highly dependent on interfacial polarisation [48]; therefore, the measurement of the dielectric constant has significant importance. For this reason, a series of measurements were performed (A-H).

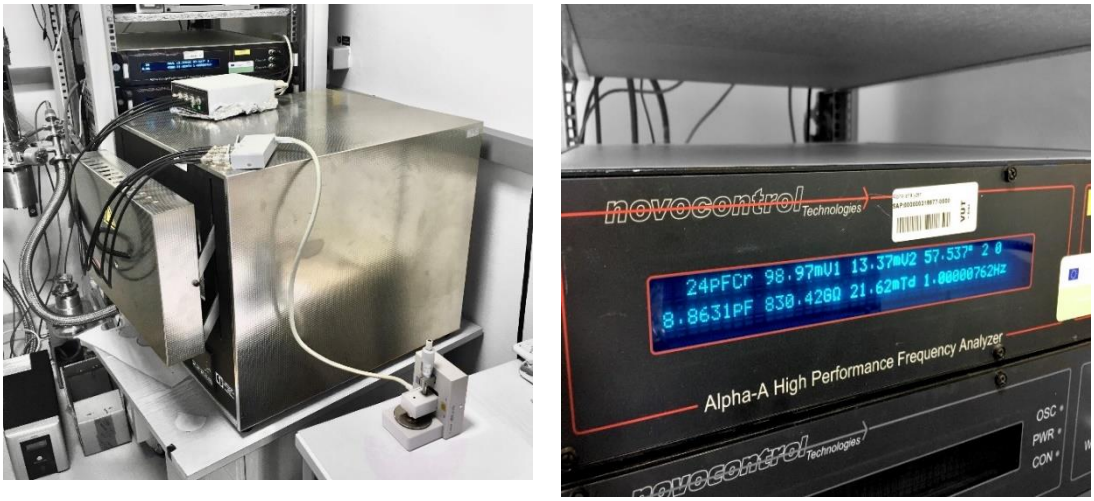

a) b)

Fig. 3.34 Alpha-A High Performance Frequency Analyser

Samples were measured in room temperature and atmospheric pressure, as the resulting sensors will be used in such conditions. Measurement was performed on Alpha-A High Performance Frequency Analyser by company Novocontrol Techniques, see Fig. 3.34. The measurement of frequency ranged from 1 Hz to 100 kHz and relative permittivity (ε_r) was measured at standard value of frequency 1000 Hz

Table 3.2 Measurement of relative permittivity (ε_r)

	BCZT	**BT**	**KNN**	**TiO_2**	**ZnO**
Relative permittivity (ε_r)	2,18	1,74	-	2,82	2,87

Higher permittivity at low frequency is connected with interfacial polarisation of the powder-polymer boundary [57]. Increasing frequency caused reducing the interactions between ions (i.e. limiting of space charges at inhomogeneities and kinetic energy of ions), leading to decreased dielectric losses. The phase ratio of the ZnO and TiO_2 doped PVDF is shown to have enhanced permittivity. It could be explained that the presence of the α-phase inside the powders allows a higher probability of domain polarisation for β and γ PVDF chains. PVDF/KNN nanocomposite could not be measured, as the sample unfortunately separated from the electrode.

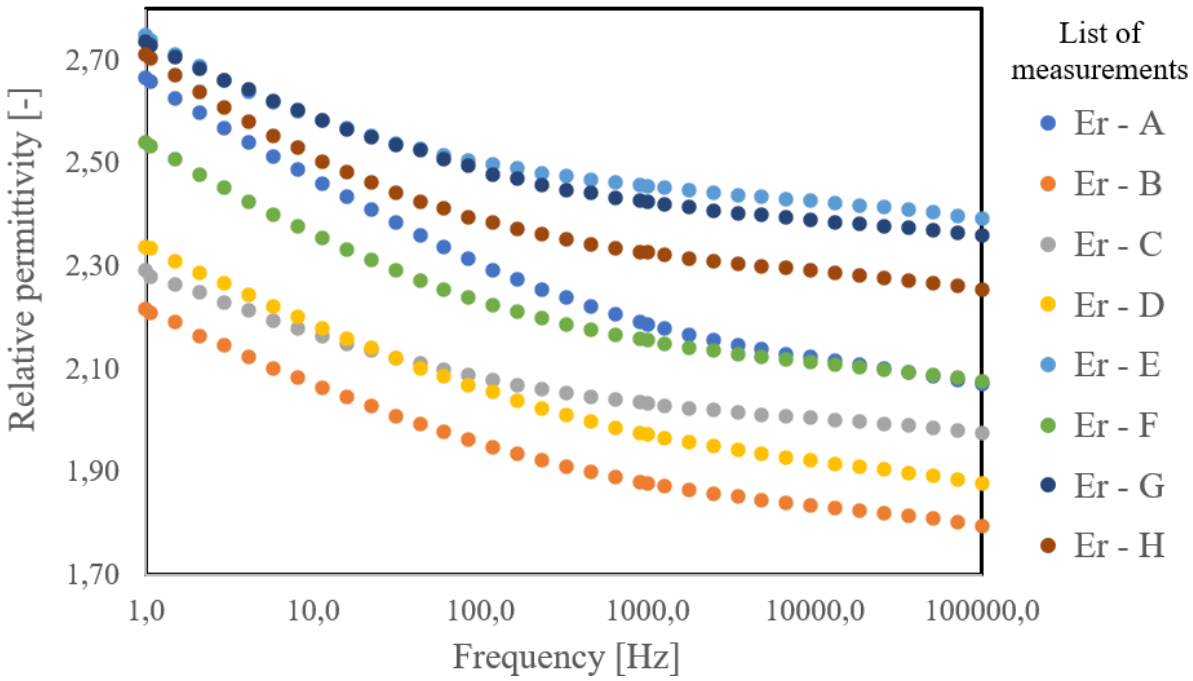

Fig. 3.35 Progress of relative permittivity of PVDF/BCZT nanocomposite in the frequency range 1-100 kHz

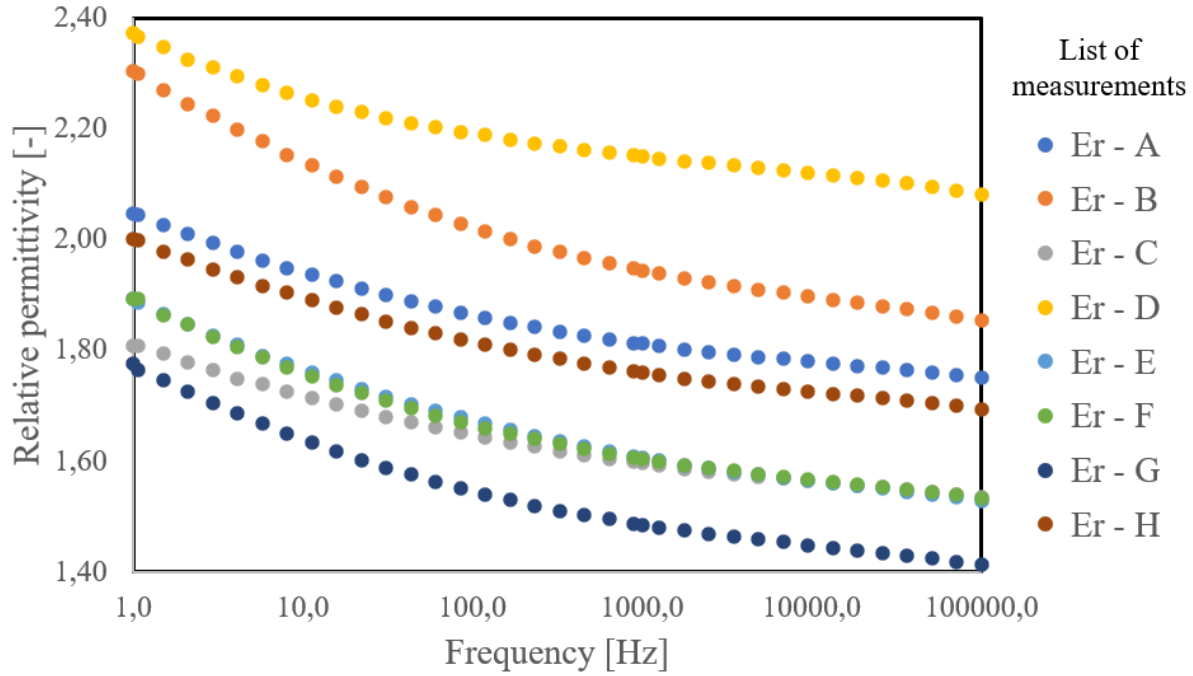

Fig. 3.36 Progress of relative permittivity of PVDF/BT nanocomposite in the frequency range 1-100 kHz

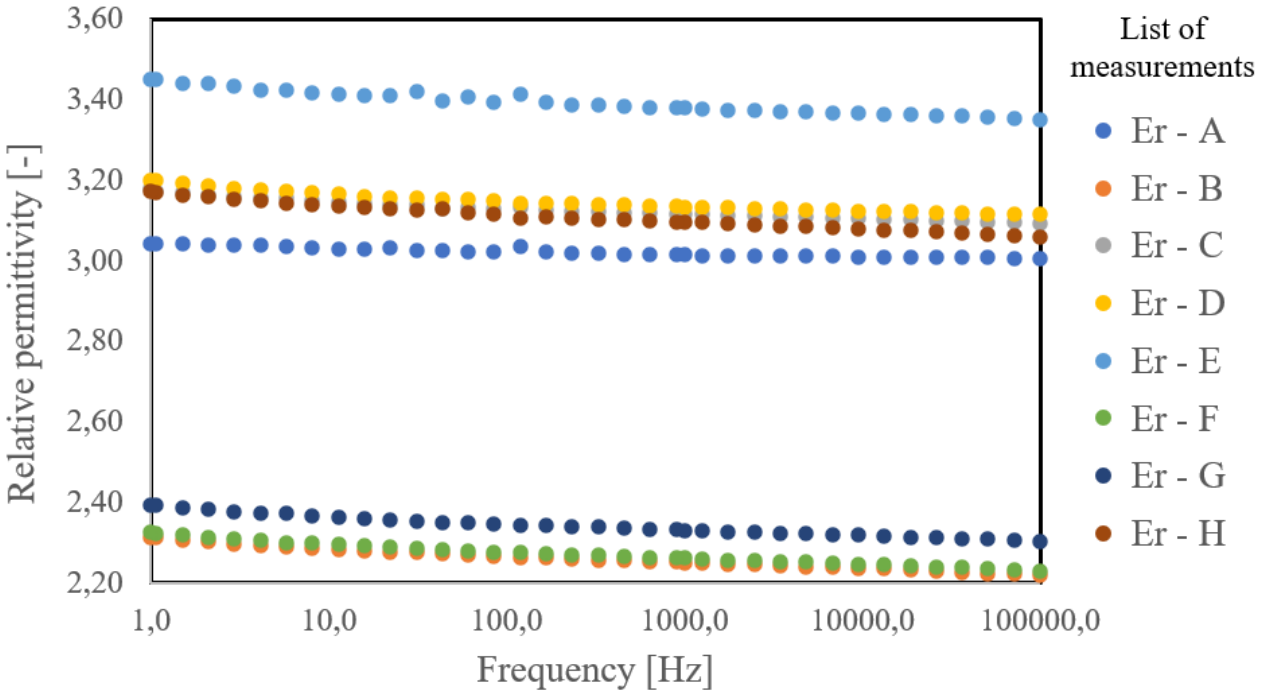

Fig. 3.37 Progress of relative permittivity of PVDF/TiO_2 nanocomposite in the frequency range 1-100 kHz

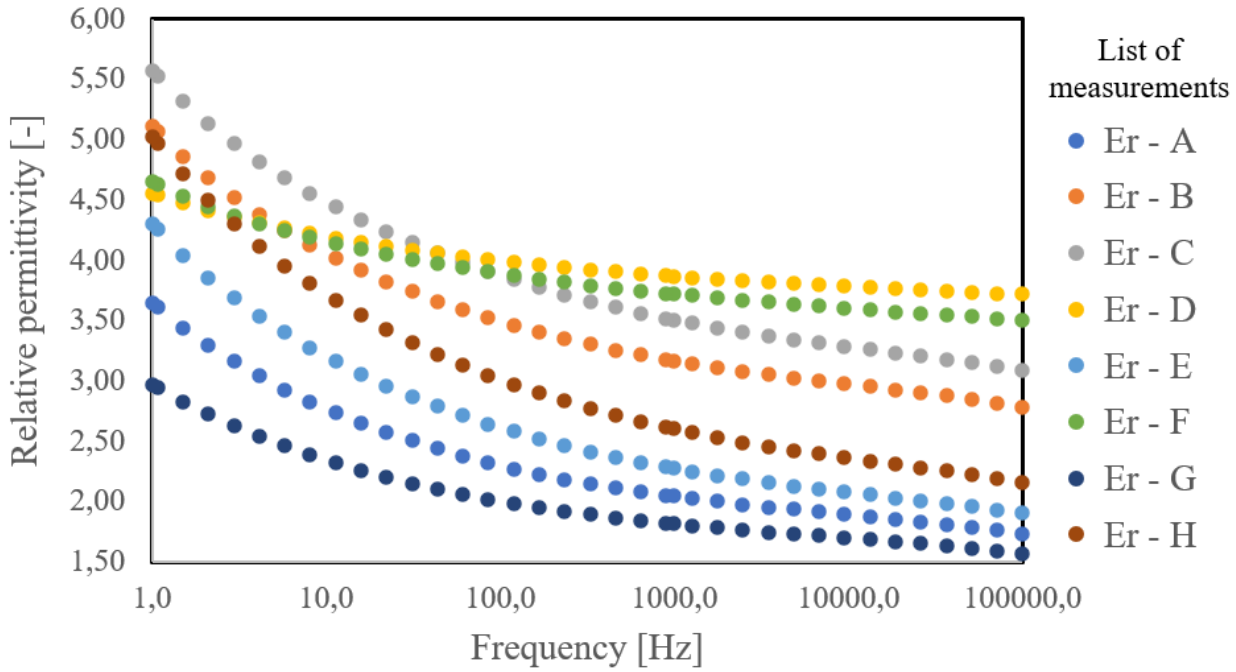

Fig. 3.38 Progress of relative permittivity of PVDF/ZnO nanocomposite in the frequency range 1-100 kHz

4. CONCLUSION

Polymer-ceramic composites can be an excellent choice to achieve miniaturisation of energy storage devices by combining the merits of polymers and ceramics. This diploma thesis describes polymers and ceramics used to form studied composites, describe fibres production, and investigate the resulting properties of those samples.

After creating the fibres from the polymer solution, the fibres' morphology was characterised by a scanning electron microscope. SEM offered a transparent picture of thin fibres enriched with ceramics particles; fibres exhibited a rough texture with a layered structure and, therefore, proposed that the ceramic particles were uniformly distributed throughout the fibres. The presence of ceramic particles in the fibres was later confirmed using energy dispersive spectroscopy. EDX provided mapping of the elements of doped ceramics using a colourful micrograph. It is possible to distinguish building elements of the doped fibres in the pictures and their even dissipation in the fibres. By exporting data from AZtech, an EDX software, it was possible to create a series of spectra, revealing the element composition in percentage. Comparison of elemental compositions of various fibres areas is sufficient evidence of satisfactory dopant distribution.

Other analyses support the EDX findings. Intermolecular interactions between different constituents of polymer nanocomposites were studied using FTIR spectroscopy. In the present study, FTIR spectroscopy was employed to explore the possible interactions between the functional groups of PVDF and nanofillers, resulting in higher peaks of β,γ-phase. In all analysed PVDF nanocomposites, additives modify the phase structure of the PVDF and the peaks associated with α-phase were significantly reduced with concurrent increased in the β-γ phase. The spectra of nanocomposites clearly suggest the successful formation of new PVDF nanocomposites.

The Raman spectra of PVDF nanocomposite fibres were supposed to provide additional data about the skeleton chain, but the β,γ phase peak is hard to distinguish in the spectra. It is because of strong luminescence background, which may be caused by the conversion of a part of the α-phase into the β-phase, as confirmed by FTIR spectra. However, the evident peak of PVDF/ZnO nanocomposite indicates enhanced performance compared to other samples.

Finally, a sequence of measurements was performed to measure the dielectric constant (relative permittivity). The dielectric constant defines the polarisation ability of the material; therefore, it is possible to directly evaluate performance of studied material. The results present significantly high values of dielectric constant in all measured samples. This verdict is undoubtly related to the structural changes as discussed above, which is an effect of enhanced β structure nucleated by ceramic nanofillers. Therefore, the enhancement was successful, and it is possible to continue with development of doped PVDF fibres.

Bibliography

[1] G. R. Mitchell, Electrospinning : Principles, Practice and Possibilities, N/A: Royal Society of Chemistry, 2015.

[2] G. G. e. a. Wallace, Conductive Electroactive Polymers : Intelligent Polymer Systems, Third ed., Boca Raton, FL: Taylor & Francis Group, 2008.

[3] K. Castkova, J. Kastyl, D. Sobola, J. Petrus, E. Stastna, D. Riha, and P. Tofel, "Structure–Properties Relationship of Electrospun PVDF Fibers," *Nanomaterials,* vol. 10, no. 6, pp. 1-19, June 2020.

[4] A. Srivastava, K. K. Jana, P. Mait and O. Parkash, "Mechanical and Dielectric Behaviour of CaCu3Ti4O12 and Nb Doped CaCu3Ti4O12 Poly(vinylidene fluoride) Composites," *Journal of Composites,* no. 769379, p. 9, 2014.

[5] A. Bharathula, "How to squeeze electricity out of crystals," 2017. [Online]. Available: https://ed.ted.com/lessons/how-to-squeeze-electricity-out-of-crystals-ashwini-bharathula#digdeeper.

[6] K. Buctela, "Gas Ionization Detectors," *Handbook of Radioactivity Analysis,* pp. 123-178, 2003.

[7] L. a. T. Li, "Electrospun Polyvinylidene Fluoride-Based Fibrous Scaffolds with Piezoelectric Characteristics for Bone and Neural Tissue Engineering," *Nanomaterials,* vol. 9, no. 7, p. 952, June 2019.

[8] Sharma, Sumeet & Chauhan, Vishal & Yadav, "A theoretical model for the electromagnetic radiation emission from ferroelectric ceramics. 14. 10.1016/j.mtcomm.2018.01.002.]," *Materials Today Communications,* vol. 14, pp. 180-187, March 2018.

[9] C. Liu, J. Shen, C. Liao, K. Yeung and S. Tjong, "Novel electrospun polyvinylidene fluoride-graphene oxide-silver nanocomposite membranes with protein and bacterial antifouling characteristics.," in *Express Polym. Lett.*, 2018.

[10] J. Y. Lim, S. Kim and Y. Seo, "Enhancement of β-phase in PVDF by electrospinning," in *AIP Conf. Proc. (Vol. 1664)*, N/A, 2015.

[11] Wu, T., Jin, H., Dong, S., Xuan, W., Xu, H., Lu, L., Luo, J., "A Flexible Film Bulk Acoustic Resonator Based on -Phase Polyvinylidene Fluoride Polymer," *Sensors (Basel),* vol. 20, no. 5, pp. 1346-1352, 29 Feb 2020.

[12] Teka, A., Bairagi, S., Shahadat, M., Joshi, M., Ziauddin Ahammad, S., & Wazed Ali, S., "Poly(vinylidene fluoride) (PVDF)/potassium sodium

niobate (KNN)-based nanofibrous web: A unique nanogenerator for renewable energy harvesting and investigating the role of KNN nanostructures," *Polym Adv Technol. ,* vol. 29(9), p. 2, 2018.

[13] Y. Li, X. Ge, L. Wang, W. Liu, H. Li, R. Li and S. Tjong, "Dielectric relaxation behavior of PVDF composites with nanofillers of different conductive nature," *Curr. Nanosci.,* no. 9, p. 679–685, 2013.

[14] S. Haddadi, S. Ghaderi, M. Amini and S. Ahmad-Ramazani, "Mechanical and piezoelectric characterizations of electrospun PVDF-nanosilica fibrous scaffolds for biomedical applications," 2018.

[15] Parjansri, P., Intatha, U., Pengpat, K. and et al. , "Improvement in the electrical properties of BCZT Ceramics induced by self-seeds," *Appl. Phys.,* 2019.

[16] Frattini, Agustin, Di Loreto and de Sanctis, "BCZT Ceramics Prepared from Activated Powders," *Materials Science,* 2012.

[17] Hajeesaeh,S., Muensit,S., "Theory and measurements for 0-3 BaTiO3," *Songklanakarin J. Sci. Technol.,* vol. 29, no. 2, pp. 413-418, May 2007.

[18] Patel, Rajkishore, Prakash, Chandra and Kumar, Pawa, "Characterizations of BT Ceramics Synthesized by Modified Solid State Route," in *AIP Conference Proceedings,* 2011.

[19] B. D. Stojanovic, V. R. Mastelaro and C. O. Paiva San, "Structure Study of Donor Doped Barium Titanate Prepared From Citrate Solutions," *Science of Sintering,* no. 179, 2004.

[20] J. Wu, "Advances in Lead-Free Piezoelectric Materials," *Springer Singapore Pte. Limited,* 2018.

[21] S. Zhangy, S. Suphankij et al, "Photocatalytic of N-doped TiO2 Nanofibers Prepared by Electrospinning," *Energy Procedia,* vol. 34, pp. 751-756, 2013.

[22] W. Z. J. Y. e. a. You H, "High-efficiency and mechano-/photo- bi-catalysis of piezoelectric-ZnO@ photoelectric-TiO2 core-shell nanofibers for dye decomposition," *Chemosphere,* no. 183, pp. 528-535, 2017.

[23] "Titanium Dioxide. Digitalfire Reference Library," [Online]. Available: https://digitalfire.com/material/titanium+dioxide.

[24] E. Gorokhova, P. Rodnyi, E. Lokshin and e. al, "Structural, optical, and scintillation characteristics of ZnO ceramics," *Journal of Optical Technology,* no. 78, pp. 753-760, 2011.

[25] U. Ozgur, Y. Alivov, C. Liu and et al., "A Comprehensive Review of ZnO Materials and Devices," *Journal of Applied Physics,* no. 98, 2005.

[26] D. Look, “Progress in ZnO materials and devices,” *Journal of Elec Materi,* no. 35, p. 1299–1305, 2006.

[27] Lu, X., Peng, Y., Qiu, H., Liu, X., Ge, L., “Anti-fouling membranes by manipulating surface wettability and their anti-fouling mechanism,” *Desalination* , vol. 413, p. 127–135, 1 July 2017.

[28] Bin Ding and et al., Electrospinning: Nanofabrication and Applications, Elsevier Science & Technology Books, 2018.

[29] Nieminen, H.J., Laidmäe, I., Salmi, A. and et al., “Ultrasound-enhanced electrospinning,” *Sci Rep 8,* no. 4437, 2018.

[30] Kanjanapongkul, K., Wongsasulak, S. and Yoovidhy, “Investigation and prevention of clogging during electrospinning of zein solution,” *J. Appl. Polym. Sci.*, no. 118, p. 1821–1829, 2010.

[31] T. Smejkalová, “Energy Dispersive X-ray spectroscopy of doped PVDF fibres,” in *Proceedings of the 27th Conference STUDENT EEICT 2021; Accepted for publication,* Brno, 2021.

[32] 4SPIN, “Electrospinning device 4SPIN,” Contipro, Milan, Italy, c2015.

[33] Microbe Notes, “Scanning Electron Microscope (SEM),” 2020.

[34] Om Prakash Choudhary and Priyanka, “Scanning Electron Microscope: Advantages and Disadvantages in Imaging Components,” *Int.J.Curr.Microbiol.App.Sci.,* pp. 1877-1882, 6 2017.

[35] CEITEC Nano Research Infrastructure, “Focused Ion Beam/Scanning Electron Microscope TESCAN LYRA3 (LYRA),” Brno.

[36] Zeppelin 3D metrology, “Tescan Lyra3/FIB,” Madrid.

[37] Thermo Fisher Scientific, “Sputter Coating for SEM: How This Sample Preparation Technique Assists Your Imaging,” 2019.

[38] Leica Microsystems, “Brief Introduction to Coating Technology for Electron Microscopy,” 2013 .

[39] Leica Mcrosystems, “Leica EM ACE,” Leica Mikrosysteme GmbH, Vienna, Austria, 2012.

[40] J. Fourie, “Gold in electron microscopy,” Gold Bull, National Physical Research Laboratory, Council for Scientific and Industrial Research, Pretoria, South Africa, 1982.

[41] Encyclopedia of Interfacial Chemistry: Surface Science and Electrochemistry, London, United Kingdom: Elsevier, 2018.

[42] S. Ebnesajjad and C. F. Ebnesajjad, Surface treatment of materials for adhesive bonding, Second ed., Amsterdam: Elsevier, 2014, p. 9780323264358.

[43] G. Webster, “Advancements in Vibrational Spectroscopy,” AZoNetwork, N/A, 2020.

[44] A. Bandyopadhyay and S. Bose, Characterization of Biomaterials, N/A: Elsevier, 2013.

[45] J. A. De Haseth, Fourier Transform Infrared Spectrometry, N/A: John Wiley & Sons, Incorporated, 2007.

[46] M. Breuer, M. Handloser and T. Gokus , “Nano-FTIR Spectroscopy Reveals Material’s True Nature,” Photonics Media, Stuttgart, 2018.

[47] Bruker, “VERTEX 70v FT-IR Spectrometer,” c2021.

[48] R. H. Upadhyay and R. R. Deshmukh, “Investigation of dielectric properties of newly prepared b-phase,” *Journal of Electrostatics,* vol. 71, pp. 945-950, 2013.

[49] Yafang Hou, Yuan Deng, Yao Wang and HongLi Gao, “Uniform distribution of low content BaTiO3 nanoparticles in poly(vinylidene fluoride) nanocomposite: Toward high dielectric breakdown strength and energy storage density,” *RSC Adv.,* vol. 5, no. 7209, August 2015.

[50] Deshmukh, K., Ahamed, M.B., Deshmukh, R.R. et al. , “Striking multiple synergies in novel three-phase fluoropolymer nanocomposites by combining titanium dioxide and graphene oxide as hybrid fillers,” *Journal of Materials Science: Materials in Electronics,* vol. 28, p. 559–575, 22 Aug 2016.

[51] K. Castkova, J. Kastyl, D. Sobola, J. Petrus, E. Stastna, D. Riha, and P. Tofel, “A critical analysis of the α, β and γ phases in poly(vinylidene fluoride) using FTIR,” *RSC Advances,* vol. 7, no. 25, pp. 15382-15389, 2017.

[52] J. Ling, S. D. Weitman, M. A. Miller and et al., “Direct Raman imaging techniques for study of the subcellular distribution of a drug,” *Applied Optics,* no. 41, pp. 6006-6017, 2002.

[53] WITec, “Correlative Raman Imaging of Semiconducting Materials,” The Analytical Scientist, 2019.

[54] B. Deepak , “What are the differences between Raman and IR Spectroscopy?,” Auriga Research Private Limited, N/A, 2015.

[55] D. Hickstein, R. Goldfarbmuren, J. Darrah, L. Erickson and L. A. Johnson, “Rapid, accurate, and precise concentration measurements of a methanol–water mixture using Raman spectroscopy,” *OSA Continuum,* vol. 1, pp. 1097-1110, 2018.

[56] Encyclopedia of Spectroscopy and Spectrometry, San Diego: Elsevier Science & Technology, 2016.

[57] CEITEC Nano Research Infrastructure, “Witec Alpha 300R (WITEC-RAMAN),” Brno, c2021.

[58] H. Peng, X. Sun, W. Weng and X. Fang, “Energy Harvesting Based on Polymer; Polymer Materials for Energy and Electronic Applications,” *Academic Press,* no. 978012811091, pp. 151-196, 2017.

[59] M. I. M. M. S. Javed, “Synthesis and characterization of TiO2 quantum dots by sol gel reflux condensation method,” *Ceram Int,* no. 45, pp. 2676-2679, 2019.

[60] Mirjalili, M. and Zohoori, S. , “Review for application of electrospinning and electrospun nanofibers technology in textile industry,” *J Nanostruct Chem,* p. 207–213, 6 2016.

[61] Spectra Research Corporation, “X-ray Photoelectron Spectroscopy (XPS),” Ontario, Canada, c2016.

[62] Physical Electronics, “XPS / ESCA,” Chanhassen, 2020.

[63] N. Gleichmann, “SEM vs TEM,” Technology Networks, N/A, 2020.

[64] “XPS / ESCA,” Physical Electronics, Inc. , Chanhassen, MN, USA, c2021.

[65] K. Naveet , T. Visalakshi and et al, “Recent Advances in Structural Health Monitoring based on EMI technique at IIT,” in *Trends and Challenges in Concrete Structures,* Ghaziabad, UP, India, 2013.

[66] A. Bunde and W. Dieterich, “Percolation in Composites,” *Journal of Electroceramics,* vol. 5, no. 2, pp. 81-92, 2000.

SYMBOLS AND ABBREVIATIONS

Abbreviations:

BCZT	Barium calcium zirconate titanate
BSE	Back-Scattered Electron
BT	Barium titanate
DLD	Delay Line Detector
DSC	Differential Scanning Calorimetry
EDS	Energy Dispersive X-Ray Spectroscopy
EDX	Energy-Dispersive X-ray
EHD	Electrohydrodynamics
ESCA	Electron Spectroscopy for Chemical Analysis
FEG	Field Emission Gun
FE-SEM	Field Emission Scanning Electron Microscopy
FIB	Focused Ion Beam
FTIR	Fourier Transform Infrared Spectroscopy
GIS	Gas Injection System
KNN	Potassium sodium niobate
MLCC	Multilayer Ceramic Capacitors
PTCR	Positive Temperature Coefficient Resistors
PVDF	Polyvinylidene fluoride
SEI	Secondary Electron Imaging
SEM	Scanning Electron Microscopy
TEM	Transmitting Electron Microscopy
TGS	Triglycine Sulphate
XPS	X-Ray Photoelectron Spectroscopy
XRD	X-Ray Diffraction